Theor Chem Acc (1998) 100:154–170
DOI 10.1007/s002149800m72

Theoretical
Chemistry Accounts

Regular article

Quenching of Li (^{2}P) by H_2: potential energy surfaces, conical intersection seam, and diabatic bases*

Eugene S. Kryachko[1], **David R. Yarkony**

Department of Chemistry, Johns Hopkins University, Baltimore, MD 21218, USA

Received: 14 August 1998 / Accepted: 20 August 1998 / Published online: 11 November 1998

Abstract. The quenching of Li $(1s^22p;{}^2\mathrm{P})$ to Li $(1s^22s;{}^2\mathrm{S})$ by H_2 is considered using coupled-cluster and multireference configuration-interaction techniques. $C_{2v}({}^2\mathrm{A}_1, {}^2\mathrm{B}_2)$ and $C_{\infty v}({}^2\Pi, {}^2\Sigma^+)$ sections of the $1^2\mathrm{A}'$ and $2^2\mathrm{A}'$ potential energy surfaces are determined. The C_{2v} portion of the $1^2\mathrm{A}' - 2^2\mathrm{A}'$ seam of conical intersection is studied. Perhaps the most significant finding is a surprising trifurcation of this seam into a portion with only C_s symmetry and the aforementioned C_{2v} portion. The adiabatic-to-diabatic state transformation is considered in the vicinity of the seam of conical intersection using both perturbation theory and the dipole moment operator. The $^2\mathrm{B}_2$ section of the $2^2\mathrm{A}'$ potential energy surface exhibits an exciplex in the general vicinity of the seam of conical intersection. The $^2\Pi$ section of the $2^2\mathrm{A}'$ potential energy surface possesses a global minimum lying 1.86 kcal/mol below the Li $(^2\mathrm{P}) + \mathrm{H}_2$ asymptote. A van der Waals-like minimum with $C_{\infty v}$ symmetry was found on the $1^2\mathrm{A}'$ potential energy surface.

Key words: Electronic quenching – Nonadiabatic coupling – Diabatic states – Conical intersection

1 Introduction

The quenching of an excited state of an atom by a diatom is an archetypical example of an electronically nonadiabatic process. The nonreactive electronic quenching reaction

$$\mathrm{Li}(1s^22p;{}^2\mathrm{P}) + \mathrm{H}_2({}^1\Sigma_g^+, v';J') \rightarrow \mathrm{LiH}_2(2^2\mathrm{A}') \rightarrow \mathrm{LiH}_2(1^2\mathrm{A}') \rightarrow \mathrm{Li}(1s^22s;{}^2\mathrm{S}) + \mathrm{H}_2({}^1\Sigma_g^+;v'',J'') \quad (1)$$

is such a process and is the focus of this work. The nonadiabatic radiationless transition $2^2\mathrm{A}' \rightarrow 1^2\mathrm{A}'$ is facilitated by a seam of conical intersection of these states which, for C_{2v} geometries, become the $1^2\mathrm{A}_1$ and $1^2\mathrm{B}_2$ states. Potential energy surfaces (PESs) for this type of reaction have been the subject of numerous theoretical studies [1–22] with the ultimate goal of understanding the nonadiabatic electronic to vibrational (v), rotational (J), and translational energy transfer. This system was also studied experimentally by Jenkins [23], Wu [24], Elward-Berry and Berry [25], and Muller and coworkers [26] (for reviews see Refs. [27, 28]). In particular, using flame fluorescence, Jenkins [23] measured the quenching cross sections of alkali atoms on diatomics and found that the cross section for quenching of the Li atom by H_2, 5.2 Å^2, is 1.8 times larger than that for Na by H_2.

The importance of conical intersections of the two lowest states of $\mathrm{Li} + \mathrm{H}_2$ in quenching process (1) was first appreciated by Krauss [1] and Tully [4, 29]. Krauss [1] calculated the four lowest potential energy curves of the $\mathrm{Li} + \mathrm{H}_2$ system in C_{2v} and $C_{\infty v}$ geometries and found crossings only for C_{2v} or T-shaped geometries (see also Ref. [10]). He also showed that, in contrast to the situation for $\mathrm{Na} + \mathrm{H}_2$, at the Hartree-Fock level, the minimal energy crossing point (MECP) of the $1^2\mathrm{A}_1$ and $1^2\mathrm{B}_2$ states of $\mathrm{Li} + \mathrm{H}_2$ is exoergic relative to Li $(^2\mathrm{P}) + \mathrm{H}_2$ [5]. A multiconfigurational self-consistent field (MCSCF) level study of the $1, 2^2\mathrm{A}'$ PESs was carried out by Matsumoto and coworkers [9–14]. They also found the MECP of the $^2\mathrm{A}_1$–$^2\mathrm{B}_2$ seam of conical intersection to be exoergic relative to the Li $(^2\mathrm{P}) + \mathrm{H}_2$ asymptote. Of particular interest in the present context is their finding [10] that an avoided intersection of the $1^2\mathrm{A}'$ and $2^2\mathrm{A}'$ states exists for $\gamma = 45°$, although at an energy higher than that of comparable C_{2v} conical intersections.

Owing to the potential of metal-doped cryogenic H_2 as a high-energy density fuel, the Li-H_2 van der Waals interaction has been a topic of recent interest (for current

* Dedicated to Prof. Dr. Wilfried Meyer on the occasion of his 60th birthday

[1]On leave from Bogoliubov Institute for Theoretical Physics, 252143 Kiev, Ukraine

Correspondence to: D. R. Yarkony

studies of $Li + H_2$ interaction relevant to the mechanism of trapping and attaching Li atoms in matrices see Refs. [30–33]). Using the method of interacting correlated fragments, Konowalow [18] determined the dissociation energy of the complex to be in the range 13–18 cm^{-1}. Chaban and Gordon [19] carried out a thorough study of the van der Waals $Li + H_2$ complex at the MP4SDQ and QCISD(T) levels with the augmented correlation-consistent valence-triple-zeta (aug-cc-pVTZ) basis set for H and the cc-pVTZ basis for Li. They found a complex with $C_{\infty v}$ symmetry stable by about 15–17 cm^{-1}.

In the present work the electronic structure aspects of reaction (1) are considered. The C_{2v} and $C_{\infty v}$ sections of the $1,2^2A'$ PESs are explored with particular emphasis on the $1^2A' - 2^2A'$ seam of conical intersection. The present treatment benefits from Meyer's important work in the area of nonadiabatic chemistry including his description of the PESs and the seam of conical intersection relevant to the quenching of Na (^2P) by H_2 [5], and from his use of the dipole moment operator to determine a transformation from an adiabatic to diabatic basis [34].

The preceding discussion has emphasized the conventional view that for reaction (1) accidental conical intersections of the $1^2A'$ and $2^2A'$ PESs occur only for C_{2v} sections where the $1^2A'$, $2^2A'$ states have $^2A_1$, $^2B_2$ symmetries while for general C_s geometries only avoided intersections are found. Quite surprisingly we will show that this conventional view of the $1^2A' - 2^2A'$ seam of conical intersection is incomplete. Rather the seam of conical intersection consists of two portions: the C_{2v} portion noted above and a portion with only C_s symmetry that intersects the C_{2v} seam producing a trifurcation [35–38]. A locally diabatic basis is constructed using the dipole moment operator and the residual derivative coupling in this basis is determined.

The remainder of the present work is organized as follows. Section 2 outlines the theoretical approach: reviewing perturbative methods for characterizing a seam of conical intersection [39] and for locating a trifurcation [37]. The relation between diabatic bases determined from derivative couplings and molecular properties operators is also considered. Section 3 presents the results of the calculations. Section 4 concludes and discusses directions for future research.

2 Conical intersections, derivative coupling, and diabatic bases

In this section, we consider the relation between the derivative couplings and approximate diabatic bases determined by requiring a molecular property to be smooth. Further, the characterization of a conical intersection, the location of a point of trifurcation, and the perturbative description of electronic dipole operator matrix elements are reviewed.

2.1 Derivative couplings and diabatic bases

The Born-Huang [40] description of a nonadiabatic process is employed here. In this approach the total wavefunction is written as a sum of the form

$$\Psi_k^T(\mathbf{r},\mathbf{R}) = \sum_{I=1}^{N^a} \chi_I^k(\mathbf{R}) e^{iA_I(\mathbf{R})} \Psi_I^a(\mathbf{r};\mathbf{R}) \equiv \boldsymbol{\chi}^k(\mathbf{R})^\dagger \tilde{\Psi}^a(\mathbf{r};\mathbf{R}) \ . \tag{2}$$

$\mathbf{r}$ denotes the coordinates of the N^e electrons and $\mathbf{R}$ the coordinates of the N^{nuc} nuclei. $\boldsymbol{\chi}(\mathbf{R})$ are the nuclear single-valued wavefunctions and $\Psi^a(\mathbf{r};\mathbf{R})$ are the N^a real-valued adiabatic electronic states. The latter are the eigenstates of the nonrelativistic Born-Oppenheimer Hamiltonian $H^e(\mathbf{r};\mathbf{R})$

$$H^e(\mathbf{r};\mathbf{R})\,\Psi_I^a(\mathbf{r};\mathbf{R}) = E_I(\mathbf{R})\Psi_I^a(\mathbf{r};\mathbf{R}) \ . \tag{3}$$

$e^{iA_I(\mathbf{R})}$ is a phase factor that accounts for the geometric phase effect [41] (for a recent review see Ref. [42] and references therein). In $\Psi_I^a(\mathbf{r};\mathbf{R})$ and $H^e(\mathbf{r};\mathbf{R})$, a semicolon separates dynamical from parametrical variables. We will suppress the $\mathbf{r}$ and/or $\mathbf{R}$ dependence of a function for clarity when no confusion results. The derivative couplings, $f_\tau^{IJ}(\mathbf{R}) \equiv \langle \Psi_I^a(\mathbf{r};\mathbf{R}) | \frac{\partial}{\partial\tau} \Psi_J^a(\mathbf{r};\mathbf{R}) \rangle_{\mathrm{r}}$, which couple $\Psi_I^a(\mathbf{r};\mathbf{R})$ in Eq. (2), satisfy

$$f_\tau^{IJ}(\mathbf{R}) = [E_I(\mathbf{R}) - E_J(\mathbf{R})]^{-1} \times \left\langle \Psi_I^a(\mathbf{r};\mathbf{R}) \middle| \frac{\partial}{\partial\tau} H^e(\mathbf{r};\mathbf{R}) \middle| \Psi_J^a(\mathbf{r};\mathbf{R}) \right\rangle_{\mathrm{r}} \tag{4}$$

where the subscript $\mathbf{r}$ denotes integration over all electronic degrees of freedom.

$\mathbf{R}_x$ is a point of conical intersection of states $I, J = I + 1$ if $E_I(\mathbf{R}_x) = E_J(\mathbf{R}_x)$ and the numerator in Eq. (4) is nonvanishing for exactly two properly chosen internal coordinates, τ_k and τ_l. In this case, there exists exactly one, again properly chosen, internal coordinate, τ_θ, for which the corresponding nonadiabatic derivative coupling $f_{\tau_\theta}^{IJ}(\mathbf{R}_x)$ is singular [39]. As a result of this singularity, it is desirable to transform to a diabatic basis [43, 44], $\Psi_I^d(\mathbf{r};\mathbf{R})$, that removes as much of the derivative coupling as possible and all the singularity.

To understand the implications of the preceding statement we restrict our attention to the case of $N^a = 2$. This case is completely adequate in the vicinity of a conical intersection and introduces no essential simplifications. The generalization to the case $N^a > 2$ can be found in Ref. [45]. In the case of $N^a = 2$, the diabatic states are obtained by orthogonal transformation of the adiabatic states:

$$\begin{pmatrix} \Psi_I^d(\mathbf{r};\mathbf{R}) \\ \Psi_J^d(\mathbf{r};\mathbf{R}) \end{pmatrix} = \begin{pmatrix} \cos\alpha(\mathbf{R}) & -\sin\alpha(\mathbf{R}) \\ \sin\alpha(\mathbf{R}) & \cos\alpha(\mathbf{R}) \end{pmatrix} \begin{pmatrix} \Psi_I^a(\mathbf{r};\mathbf{R}) \\ \Psi_J^a(\mathbf{r};\mathbf{R}) \end{pmatrix} \tag{5}$$

which we abbreviate as $\Psi^d = \mathbf{u}(\alpha)\Psi^a$, where $\alpha(\mathbf{R})$ is the adiabatic-to-diabatic states mixing angle. The above goals will certainly be met if we require for all τ

$$f_\tau^{d,IJ}(\mathbf{R}) \equiv \left\langle \Psi_I^d(\mathbf{r};\mathbf{R}) \middle| \frac{\partial}{\partial\tau} \Psi_J^d(\mathbf{r};\mathbf{R}) \right\rangle_{\mathrm{r}} = f_\tau^{IJ}(\mathbf{R}) + \frac{\partial}{\partial\tau}\alpha(\mathbf{R}) = 0 \ , \tag{6}$$

where $f_\tau^{d,IJ}$ is the derivative coupling in diabatic basis. The basis that obeys Eq. (6) is referred to as strictly diabatic. The formal solution of Eq. (6) is straightforward,

$$\alpha(\mathbf{R}) = \alpha(\mathbf{R}_0) + \int_{\mathrm{R}_0}^{\mathrm{R}} \mathbf{f}^{IJ} \cdot d\mathbf{R} \ . \tag{7}$$

$\alpha(\mathbf{R}_0)$ is the initial value of the mixing angle. Equation (6) is seen to require that $\mathbf{f}^{IJ}$ be the gradient of a scalar. Then for Eq. (6) to be solvable, the curl of $\mathbf{f}^{IJ}$ must vanish or equivalently the mixed second partial derivatives of $\alpha(\mathbf{R})$ must be equal, that is:

$$\frac{\partial^2}{\partial\tau_k\partial\tau_l}\alpha(\mathbf{R}) - \frac{\partial}{\partial\tau_l\partial\tau_k}\alpha(\mathbf{R}) = \frac{\partial}{\partial\tau_k} f^{IJ}_{\tau_l}(\mathbf{R}) - \frac{\partial}{\partial\tau_l} f^{IJ}_{\tau_k}(\mathbf{R}) \ = 0 \ . \tag{8a}$$

The second condition in Eq. (8a) yields

$$\left\langle \frac{\partial}{\partial\tau_k}\Psi^a_I \middle| \frac{\partial}{\partial\tau_l}\Psi^a_J \right\rangle_{\mathrm{r}} - \left\langle \frac{\partial}{\partial\tau_l}\Psi^a_I \middle| \frac{\partial}{\partial\tau_k}\Psi^a_J \right\rangle_{\mathrm{r}} = \sum_{K\neq I,J} \left(f^{KI}_{\tau_k} f^{KJ}_{\tau_l} - f^{KI}_{\tau_l} f^{KJ}_{\tau_k} \right) = 0 \ . \tag{8b}$$

McLachlan [46, 47] and Baer [48] first noted the requirement expressed in Eq. (8a). Mead and Truhlar [45] proved that, in general, the requirement expressed by Eq. (8b) is not satisfied. Since the curl of $\mathbf{f}^{IJ}$ does not vanish, the integral of $\mathbf{f}^{IJ}$ is path dependent and $\alpha(\mathbf{R})$ cannot be determined by Eq. (7).

Note that

$$\sum_{K\neq I,J} \left(f^{KI}_{\tau_k} f^{KJ}_{\tau_l} - f^{KI}_{\tau_l} f^{KJ}_{\tau_k} \right) = \sum_{K\neq I,J} \left(\frac{\left\langle \Psi^a_I \middle| \frac{\partial}{\partial\tau_k} H^e \middle| \Psi^a_K \right\rangle_{\mathrm{r}} \left\langle \Psi^a_J \middle| \frac{\partial}{\partial\tau_l} H^e \middle| \Psi^a_K \right\rangle_{\mathrm{r}} - \left\langle \Psi^a_I \middle| \frac{\partial}{\partial\tau_l} H^e \middle| \Psi^a_K \right\rangle_{\mathrm{r}} \left\langle \Psi^a_J \middle| \frac{\partial}{\partial\tau_k} H^e \middle| \Psi^a_K \right\rangle_{\mathrm{r}}}{[(E_K - E_I)(E_K - E_J)]} \right) \ , \tag{8c}$$

so that although $\mathbf{f}^{IJ}$ is singular at a conical intersection, its curl is not.

2.2 Molecular properties and diabatic bases

An alternative to Eq. (7) for the determination of the adiabatic-to-diabatic mixing angle $\alpha(\mathbf{R})$ is based on the suggestion of Werner and Meyer [34] (see also Macías and Riera [49, 50] and Refs. [51–60]) that the matrix elements of the electronic dipole moment operator be used to determine $\alpha(\mathbf{R})$ avoiding entirely the use of derivative couplings. In order to see the connection between this suggestion and the above definition of the diabatic basis, $\mathbf{f}^{d,IJ} = 0$, we consider an arbitrary real-valued Hermitian electronic operator $A(\mathbf{r})$ depending solely on the electronic variables. Its matrix elements in the adiabatic basis are $A_{IJ}(\mathbf{R}) \equiv \langle \Psi^a_I(\mathbf{r};\mathbf{R}) \,|\, A(\mathbf{r}) \Psi^a_J(\mathbf{r};\mathbf{R}) \rangle_{\mathrm{r}}$, so for each τ we obtain an "equation of motion",

$$\frac{\partial}{\partial\tau}\mathbf{A}(\mathbf{R}) = [\mathbf{A}(\mathbf{R}), \mathbf{F}^{\tau}(\mathbf{R})] \ , \tag{9}$$

where, in terms of the Pauli matrices $\boldsymbol{\sigma}_w$,

$$\mathbf{A}(\mathbf{R}) = A^+(\mathbf{R})\mathbf{I} + A^-(\mathbf{R})\boldsymbol{\sigma}_z + A_{IJ}(\mathbf{R})\boldsymbol{\sigma}_x \tag{10a}$$

$$\mathbf{F}^{\tau}(\mathbf{R}) = \mathrm{i} f^{IJ}_{\tau}(\mathbf{R})\boldsymbol{\sigma}_y \tag{10b}$$

with $A^{\pm} = (A_{II} \pm A_{JJ})/2$. Therefore, Eq. (9) can be rewritten as

$$\frac{\partial}{\partial\tau}\mathbf{A}(\mathbf{R}) = 2f^{IJ}(\mathbf{R})[A^-(\mathbf{R})\boldsymbol{\sigma}_x - A_{IJ}(\mathbf{R})\boldsymbol{\sigma}_z] \ . \tag{10c}$$

Using Eq. (10a) in Eq. (10c) gives

$$\frac{\partial}{\partial\tau}A^+(\mathbf{R}) = 0, \quad \frac{\partial}{\partial\tau}A_{IJ}(\mathbf{R}) = 2f^{IJ}(\mathbf{R})A^-(\mathbf{R}) \text{ and}$$
$$\frac{\partial}{\partial\tau}A^-(\mathbf{R}) = -2f^{IJ}(\mathbf{R})A_{IJ}(\mathbf{R}) \ . \tag{11}$$

Assume that Eq. (8b) is valid. This turns out to be effectively the case near a conical intersection [see Ref. [61] and the comment following Eq. (8c)]. We wish to obtain a new basis, $\tilde{\Psi} = \mathbf{u}(\beta)\Psi^a$ such that the smoothness property $\frac{\partial}{\partial\tau}\tilde{\mathbf{A}} = \mathbf{0}$ is satisfied. From Eq. (10a) and the definition of $\tilde{\Psi}$, we obtain

$$\tilde{\mathbf{A}}(\mathbf{R}) = \mathbf{u}(\beta)\mathbf{A}\mathbf{u}^{\dagger}(\beta) = A^+\mathbf{I} + (A^-\cos 2\beta - A_{IJ}\sin 2\beta)\boldsymbol{\sigma}_z + (A^-\sin 2\beta - A_{IJ}\cos 2\beta)\boldsymbol{\sigma}_x \ . \tag{12}$$

Then differentiating Eq. (12) and using Eq. (11), we derive

$$\frac{\partial}{\partial\tau}\tilde{\mathbf{A}}(\mathbf{R}) = \left(\frac{\partial}{\partial\tau}\tilde{A}^+\right)\mathbf{I} + \left(\frac{\partial}{\partial\tau}\tilde{A}^-\right)\boldsymbol{\sigma}_z + \left(\frac{\partial}{\partial\tau}\tilde{A}_{IJ}\right)\boldsymbol{\sigma}_x = -2\left(f^{IJ}_{\tau} + \frac{\partial}{\partial\tau}\beta\right)[(A_{IJ}\cos 2\beta + A^-\sin 2\beta)\boldsymbol{\sigma}_z + (A_{IJ}\sin 2\beta - A^-\cos 2\beta)\boldsymbol{\sigma}_x] = 0 \ . \tag{13}$$

Thus, Eq. (13) is satisfied provided $\beta = \alpha$. This key result establishes the sense in which diabatic bases give rise to smooth molecular properties.

Equation (13) also suggests:

$$\tan 2\beta_{\kappa}(\mathbf{R}) = \frac{A_{IJ}\cos 2\kappa + A^-\sin 2\kappa}{A_{IJ}\sin 2\kappa - A^-\cos 2\kappa} \tag{14a}$$

$$= 2\bar{A}_{IJ}(\mathbf{R})/[\bar{A}_{JJ}(\mathbf{R}) - \bar{A}_{II}(\mathbf{R})], \tag{14b}$$

where κ is an arbitrary angle. Here $\bar{A}_{IJ}(\mathbf{R}) \equiv \langle \bar{\Psi}^a_I(\mathbf{r};\mathbf{R}) | A(\mathbf{r}) | \bar{\Psi}^a_J(\mathbf{r};\mathbf{R}) \rangle_{\mathrm{r}}$ and $\bar{\Psi}^a = \mathbf{u}(\kappa)\Psi^a$. Explicit differentiation of Eq. (14a) shows that $\beta_{\kappa}(\mathbf{R})$ satisfies Eq. (6) provided Eq. (9) holds.

Equation (14a) provides a generalization of the angle α^{WM} which Werner and Meyer [34] proposed to define an adiabatic-to-diabatic basis transformation via Eq. (5). $\alpha^{\mathrm{WM}} = \beta_{\kappa=0}$ with $A = \mu^w$, the wth component of the electronic dipole moment operator ($w = x$, y, or z). Since β_{κ} diagonalizes $\bar{\mathbf{A}}(\mathbf{R})$, the $\kappa \neq 0$ result can be

viewed as diagonalizing, not **A** constructed in the adiabatic states basis as suggested by Werner and Meyer [34], but rather **A** constructed in a basis that differs by a fixed rotation of the adiabatic basis. $\beta_{\kappa\neq 0}$ produces a diabatic basis that has a nonzero transition dipole moment. We will return to Eq. (14) in Sect. 3.6.

2.3 Conical intersections and intersecting seams

Near a conical intersection not all sets of nuclear coordinates are equivalent. We define a particular optimal set of coordinates [39] and recapitulate their relation to the location of intersecting seams of conical intersection [37].

$\Psi_I^a(\mathbf{r};\mathbf{R})$ are expanded in a basis:

$$\Psi_I^a(\mathbf{r};\mathbf{R}) = \sum_{\alpha=1}^{N^{\mathrm{CSF}}} \mathbf{c}_\alpha^I(\mathbf{R})\psi_\alpha(\mathbf{r};\mathbf{R}) \ . \tag{15a}$$

$\mathbf{c}^I(\mathbf{R})$ satisfy

$$[\mathbf{H}(\mathbf{R}) - E_I(\mathbf{R})]\mathbf{c}^I(\mathbf{R}) = 0 \ . \tag{15b}$$

In the numerical treatment described below, ψ_α will be configuration state functions (CSFs) [62] constructed from molecular orbitals which are obtained from a state-averaged MCSCF (SA-MCSCF) procedure [62].

To analyze the neighborhood of $\mathbf{R}_x$, a point of conical intersection of the states I and $J = I + 1$, it is convenient to introduce a generalized cylindrical polar coordinate system: with origin at $\mathbf{R}_x$; an $x-y$ or $\mathbf{g}-\mathbf{h}(\mathbf{R}_x)$ plane defined by the vectors $\mathbf{g}^{IJ}(\mathbf{R}_x)$ and $\mathbf{h}^{IJ}(\mathbf{R}_x)$, and a subspace orthogonal to the $\mathbf{g}-\mathbf{h}(\mathbf{R}_x)$ plane, $\mathbf{g}-\mathbf{h}^\perp(\mathbf{R}_x)$, with the axes $\mathbf{z}^i$, $i = 3 - N^{\mathrm{int}}$. Here

$$2g_\tau^{IJ}(\mathbf{R}) = [\mathbf{c}^I(\mathbf{R}_x) - \mathbf{c}^J(\mathbf{R}_x)]^\dagger \frac{\partial \boldsymbol{H}(\mathbf{R})}{\partial \tau}[\mathbf{c}^J(\mathbf{R}_x) + \mathbf{c}^J(\mathbf{R}_x)] \ , \tag{16a}$$

$$h_\tau^{IJ}(\mathbf{R}) = \mathbf{c}^I(\mathbf{R}_x)^\dagger \frac{\partial \boldsymbol{H}(\mathbf{R})}{\partial \tau}\mathbf{c}^J(\mathbf{R}_x) \ , \tag{16b}$$

and N^{int} is the number of internal nuclear coordinates. It is also useful to define the vector

$$2s_\tau^{IJ}(\mathbf{R}) = [\mathbf{c}^I(\mathbf{R}_x) + \mathbf{c}^J(\mathbf{R}_x)]^\dagger \times \frac{\partial \boldsymbol{H}(\mathbf{R})}{\partial \tau}[\mathbf{c}^I \ \mathbf{R}_x) + (\mathbf{c}^J(\mathbf{R}_x)] - 2\,h_\tau^{IJ}(\mathbf{R}) \ . \tag{16c}$$

The $\mathbf{g}-\mathbf{h}(\mathbf{R}_x)$ plane is perpendicular to the tangent to the seam of conical intersection. The x-axis is chosen along the unit vector $\hat{\mathbf{x}} = \mathbf{h}^{IJ}(\mathbf{R}_x)/\|\mathbf{h}^{IJ}(\mathbf{R}_x)\|$ while the unit vector $\hat{\mathbf{y}} = \mathbf{g}^{IJ}(\mathbf{R}_x)^\perp/\|\mathbf{g}^{IJ}(\mathbf{R}_x)^\perp\|$ determines the y-axis, where $\mathbf{g}^{IJ}(\mathbf{R}_x)^\perp = \mathbf{g}^{IJ}(\mathbf{R}_x) - [\mathbf{g}^{IJ}(\mathbf{R}_x)^\dagger \cdot \hat{\mathbf{x}}]\hat{\mathbf{x}}$. The polar coordinates $(\rho,\ \theta)$ are defined by $x = \rho\cos\theta$ and $y = \rho\sin\theta$. In the case of a three-atom system, the dimension of $\mathbf{g}-\mathbf{h}^\perp(\mathbf{R}_x)$ is 1 and $\mathbf{z}^3$ is chosen as the unit vector parallel to $\mathbf{t}^{IJ}[\mathbf{R}_x] = \mathbf{g}^{IJ}[\mathbf{R}_x] \times \mathbf{h}^{IJ}(\mathbf{R}_x)$. Note that $\mathbf{t}^{IJ}$ is uniquely determined [37] (except as discussed below) although $\mathbf{g}^{IJ}(\mathbf{R}_x)$ and $\mathbf{h}^{IJ}(\mathbf{R}_x)$ are not. This later observation is a consequence of the degeneracy $E_I(\mathbf{R}_x) = E_J(\mathbf{R}_x)$, at $\mathbf{R}_x$ which leaves $\mathbf{c}^J(\mathbf{R}_x)$ and $\mathbf{c}^J(\mathbf{R}_x)$ defined only to within an arbitrary rotation.

$\mathbf{R}_x$ is a point of conical intersection provided $\mathbf{g}^{IJ}(\mathbf{R}_x)$ and $\mathbf{h}^{IJ}(\mathbf{R}_x)$ are linearly independent. Significantly, if $\mathbf{g}^{IJ}(\mathbf{R}_x)$ and $\mathbf{h}^{IJ}(\mathbf{R}_x)$ are not linearly independent, so that $\|\mathbf{t}^{IJ}[\mathbf{R}_x]\| = 0$, then $\mathbf{R}_x$, although not a point of conical intersection, may be a point of intersection of two seams of conical intersection [37]. This observation is used later in Sect. 3.2.

In the neighborhood of $\mathbf{R}_x$, it is convenient to replace the CSF basis with an alternative basis, $\tilde{\psi}_I(\mathbf{r};\mathbf{R})$ analogous to the crude adiabatic basis of Longuet-Higgins [63]:

$$\tilde{\psi}_I\ (\mathbf{r};\mathbf{R}) = \sum_{\alpha=1}^{N^{\mathrm{CSF}}} c_\alpha^I(\mathbf{R}_x)\psi_\alpha(\mathbf{r};\mathbf{R}) \tag{17a}$$

so that

$$\Psi_I(\mathbf{r};\mathbf{R}) = \sum_{K=I,J} \xi_K^I(\mathbf{R})\tilde{\psi}_K(\mathbf{r};\mathbf{R}) + \sum_{K\neq I,J} \Xi_K^I(\mathbf{R})\tilde{\psi}_K(\mathbf{r};\mathbf{R}) \ . \tag{17b}$$

Then, at $\mathbf{R} = \mathbf{R}_x + \delta\mathbf{R}$, $\boldsymbol{\xi}$ and $\boldsymbol{\Xi}$ can be expanded in a power series in $\delta\mathbf{R}$ as follows:

$$\boldsymbol{\xi}^I(\mathbf{R}) \cong \tilde{\boldsymbol{\xi}}^{0,I}(\theta) + \boldsymbol{\xi}^{1,I}(\mathbf{R}) + \cdots \tag{18a}$$

$$\boldsymbol{\Xi}^I(\mathbf{R}) \cong \boldsymbol{\Xi}^{1,I}(\mathbf{R}) + \cdots \ , \tag{18b}$$

where [39] $\tilde{\boldsymbol{\xi}}^0(\theta) = \mathbf{u}(\lambda(\theta)/2)\boldsymbol{\xi}^0(\mathbf{R}_x)$ and $\xi_K^{0,I}(\mathbf{R}_x) = \delta_{KI}$ and

$$\begin{aligned} q(\theta)\cos\lambda(\theta) &= g_x\cos\theta + g_y\sin\theta, \\ q(\theta)\sin\lambda(\theta) &= h_x\cos\theta \end{aligned} \tag{19a}$$

$$q(\theta)^2 = h_x^2\cos^2\theta + (g_x\cos\theta + g_y\sin\theta)^2 \ . \tag{19b}$$

To first order in displacement $\delta\mathbf{R}$ from $\mathbf{R}_x$,

$$E_I(\mathbf{R}) \approx E_I^{(p1)}(\mathbf{R}) \equiv \mathbf{s}^{IJ}\cdot\delta\mathbf{R} - \rho q(\theta) \ . \tag{20}$$

Furthermore, one may show that for ρ sufficiently small, $\beta_{\kappa=0}$ is given by [60]

$$2\beta_{\kappa=0}(\theta) + \delta + \lambda(\theta) = n\,\pi, \quad n = 0, \pm 1, \ldots \tag{21}$$

where the offset angle, δ, satisfies $\tan\delta = A_{IJ}/A^-$.

Equation (21) [60] is a key result for the following reasons. To first order in perturbation theory, $\alpha(\mathbf{R}) = \alpha^{(\mathrm{p1})}(\mathbf{R}) = -\lambda(\theta)/2$ [39]. $\alpha^{(\mathrm{p1})}$ is relevant to the definition of diabatic states in terms of derivative coupling, Eq. (6), in the following sense. It can be shown [39, 64] that $(1/\rho)\frac{\partial}{\partial\theta}\alpha^{(\mathrm{p1})}(\mathbf{R}) \equiv (1/\rho)f_\theta^{(\mathrm{p1})}$ exactly cancels the only singular part of the derivative coupling, $(1/\rho)f_\theta^{IJ}(\mathbf{R})$, at $\mathbf{R}_x$. The remaining components of the derivative coupling, f_ρ^{IJ} and $f_{z^i}^{IJ}$, are nonsingular at $\mathbf{R}_x$. Thus near a conical intersection, Eq. (21) provides the bridge between a diabatic basis based on derivative couplings, $\alpha = \alpha^{(\mathrm{p1})}$, and a molecular-property-based diabatic basis, $\alpha = \beta_\kappa$. In fact, it follows from Eq. (21) that the property-based transformation proposed by

Werner and Meyer [34] removes completely the singularity in the derivative coupling at $\mathbf{R}_x$ [60].

Finally note that perturbation theory also yields a useful estimate for the dipole and transition dipole moments in the vicinity of a conical intersection [60]:

$$\boldsymbol{\mu}(\rho \to 0, \theta, z^i = 0) \equiv \boldsymbol{\mu}^{(\mathrm{p0})}(\theta) = \mu^+ \mathbf{I} + \boldsymbol{\sigma}_x(\mu^- \sin\lambda + \mu_{IJ}\cos\lambda) + \boldsymbol{\sigma}_z(\mu^- \cos\lambda - \mu_{IJ}\sin\lambda) \tag{22}$$

where $\mu^{\pm} = [\mu_{II}(\mathbf{R}_x) \pm \mu_{JJ}(\mathbf{R}_x)]/2$ and $\boldsymbol{\mu}_{KL}(\mathbf{R}) \equiv \langle \Psi_K^a(\mathbf{r};\mathbf{R}) | \boldsymbol{\mu}^{\mathrm{e}}(\mathbf{r}) | \Psi_L^a(\mathbf{r};\mathbf{R}) \rangle_r$.

3 Li + H_2 PESs and their conical intersections

3.1 Computational prerequisities

The geometry of the Li + H_2 complex is specified by the standard three-body Jacobi coordinates $\mathbf{R} = (R, r, \gamma)$ where $r = R$(H-H). The electronic structure calculations are performed at two levels. The seam of conical intersection is characterized using second-order configuration interaction wave functions based on a three-electron, $(5a', 1a'')$ orbital active space. In the asymptotic region this active space is formed by the Li $(2s, 2p)$ and H$(1s)$ orbitals. The molecular orbitals are determined from a SA-MCSCF procedure that averages the $1, 2^2\mathrm{A}'$ and $1^2\mathrm{A}''$ states with weights 0.51, 0.49, and 0.5, respectively, and employs a $[8s3p1d]/(6s3p1d)$ basis set [65] on H atoms and a $(9s8p2d)$basis on Li [18]. At this level $N^{\mathrm{CSF}} = 23877$.

The PESs are surveyed, and van der Waals structures are determined, at the CCSD(T)/cc-pVQZ level, which consists of spin-unrestricted coupled-cluster CCSD(T) wavefunctions [66] based on the augmented correlation-consistent valence-quadruple-zeta (aug-cc-pVQZ) basis set of Dunning [67] for H and a cc-pVQZ basis for Li, yielding $N^{\mathrm{CSF}} = 17565$. As in the case of the MCSCF/CI wavefunctions, the 1*s* orbital on the Li atom is not correlated. In the asymptotic region, $\mathbf{R}_{\mathrm{asym}} = (50, 1.4011, \gamma)$ one obtains $E_{1^2\mathrm{A}'}(\mathbf{R}_{\mathrm{asym}}) = -8.6055930$ and $E_{2^2\mathrm{A}'}(\mathbf{R}_{\mathrm{asym}}) = -8.5378618$ hartree using MCSCF/CI wavefunctions. These values are only 197.2 and 211.5 cm^{-1} higher than $E_{1^2\mathrm{A}'}(\mathbf{R}_{\mathrm{asym}}) = -8.60649151$ and $E_{2^2\mathrm{A}'}(\mathbf{R}_{\mathrm{asym}}) = -8.53882546$ hartree determined at the CCSD(T)/cc-pVQZ level. Subsequent comparisons will serve to confirm the approximate equivalence of the MCSCF/CI and CCSD(T) treatments suggested by this comparison. The results at $\mathbf{R}_{\mathrm{asym}}$ imply $\Delta E(^2\mathrm{S} \to {}^2\mathrm{P}) = 1.843[1.841]$ eV at the MCSCF/CI[CCSD(T)] level which is in excellent agreement with the experimental value 1.848 eV [68]. For the remainder of this work energies will be expressed relative to the corresponding $E_{1^2\mathrm{A}'}(\mathbf{R}_{\mathrm{asym}})$ unless otherwise noted.

At the CCSD(T)/cc-pVQZ level, a van der Waals-like minimum was found on the $1^2\mathrm{A}'$ PES at the $C_{\infty v}$ structure $\mathbf{R}_{\mathrm{vm}} = (9.37, 1.4011, 0^\circ)$ with $E_{1^2\mathrm{A}'}(\mathbf{R}_{\mathrm{vm}}) = 11.3\,\mathrm{cm}^{-1}$ (taking a basis set superposition error of $0.9\,\mathrm{cm}^{-1}$ into account). This structure is displayed in Fig. 1. The results are in good accord with the recent study of Chaban and Gordon [19] who report a collinear van der Waals minimum at $\mathbf{R}_{\mathrm{vm}}^{\mathrm{CG}} = (9.845, 1.402, 0^\circ)$ with an energy $E_{1^2\mathrm{A}'}(\mathbf{R}_{\mathrm{vm}}^{\mathrm{CG}}) = 15\,\mathrm{cm}^{-1}$. Also found was a van der Waals-like saddle point on the ground-state PES for the perpendicular configuration $\mathbf{R}_{\mathrm{vts}} = (10.66, 1.4011, 90^\circ)$ with $E_{1^2\mathrm{A}'}(\mathbf{R}_{\mathrm{vts}}) = 5.6\,\mathrm{cm}^{-1}$, again in good accord with the results of Gordon and Chaban, $\mathbf{R}_{\mathrm{vts}}^{\mathrm{CG}} = (10.204, 1.402, 90^\circ)$ with $E_{1^2\mathrm{A}'}(\mathbf{R}_{\mathrm{vts}}^{\mathrm{CG}}) = 9\,\mathrm{cm}^{-1}$.

The focus of this work is the nonadiabatic quenching of Li (^{2}P) by H_2. In order to orient the presentation we begin by discussing the locus of the $1^2\mathrm{A}' - 2^2\mathrm{A}'$ seam of conical intersection. In subsequent sections, we analyze the conical intersections and discuss paths to the region of conical intersection.

3.2 LiH_2 $1^2A' - 2^2A'$ conical intersections

3.2.1 The C_{2v} portion

The C_{2v} region of the conical intersection seam between the states $1^2\mathrm{A}'$ and $2^2\mathrm{A}'$ is readily anticipated. Table 1 tabulates the points, $\mathbf{R}_x$, which satisfy $[E_{1^2\mathrm{A}'}(\mathbf{R}_x) - E_{2^2\mathrm{A}'}(\mathbf{R}_x)] < 0.02\,\mathrm{cm}^{-1}$. On the C_{2v} seam, $\mathbf{R}_x$ is parameterized by r so that $\mathbf{R}_x^{\mathrm{C2v}}(r) = (\mathbf{R}(r), r, 90^\circ)$. The superscript C2v will be suppressed when no confusion resuts. $E[\mathbf{R}_x(r)] \equiv E_{1^2\mathrm{A}'}(\mathbf{R}_x(r))$ as function of r is displayed in Fig. 2 and tabulated in Table 1. All $\mathbf{R}_x(r)$ with $1.5\ a_0 < r < 2.2\,a_0$ are exoergic relative to the reactant asymptote of quenching process (1), i.e., $E_{1^2\mathrm{A}'}(\mathbf{R}_x(r)) < E_{2^2\mathrm{A}'}(\mathbf{R}_{\mathrm{asym}})$ for such values of r. This portion of the C_{2v} crossing seam becomes accessible only if the H_2 bond is stretched or diluted providing a manifestation of the bond-stretch attraction or bond-dilution mechanism discussed by Hertel [28] (see also Ref. [69] and references therein). For R(H-H) $\geq 2.3\,a_0$ the crossing point occurs for longer R and the crossing energy lies above the reactant asymptote $E_{2^2\mathrm{A}'}(\mathbf{R}_{\mathrm{asym}})$.

The MECP on the $1^2\mathrm{A}' - 2^2\mathrm{A}'$ C_{2v} seam of conical intersection is $\mathbf{R}_x(1.77) \equiv \mathbf{R}_{\mathrm{mex}} = (2.969, 1.770, 90.0^\circ)$, where $E(\mathbf{R}_{\mathrm{mex}}) = 1.124$ eV and is exoergic with respect to $E_{2^2\mathrm{A}'}(\mathbf{R}_{\mathrm{asym}})$ by $\sim$0.7 eV. $\mathbf{R}_{\mathrm{mex}}$ is in qualitative agreement with the results of Matsumoto et al. [9–14], $\mathbf{R}_{\mathrm{mex}} = (2.9344, 1.9530, 90^\circ)$ [11], and Saxe and Yarkony [70], $\mathbf{R}_{\mathrm{mex}} = (3.0, 1.9, 90^\circ)$, and is in satisfactory accord with the more recent result of Martinez [20], $\mathbf{R}_{\mathrm{mex}} = (2.86 \pm 0.01, 1.78 \pm 0.01, 90^\circ)$.

Table 1 reports and Fig. 2 depicts $\pm||\mathbf{t}^{IJ}[\mathbf{R}_x(r)]||$ along the seam of conical intersection. The sign convention is discussed in Ref. [37]. In Fig. 2 it is seen that $||\mathbf{t}^{IJ}[\mathbf{R}_x(r)]||$ attains a maximum at the crossing point $\mathbf{R}_x(2.57) = (4.43, 2.57, 90^\circ)$ for which the energy $E[\mathbf{R}_x(2.57)] = 2.48$ eV. Figure 2 also demonstrates that $||\mathbf{t}^{IJ}[\mathbf{R}_x(r)]||$ approaches zero in a linear manner as r approaches 1.28 a_0, and also for large r, about 5.0 a_0. The vanishing of $||\mathbf{t}^{IJ}[\mathbf{R}_x(r)]||$ for large r (and large R) reflects the (nonconical) degeneracy of Li + H + H configurations and is of little interest here. However, the vanishing of $||\mathbf{t}^{IJ}[\mathbf{R}_x(r)]||$ at $r = 1.28\,a_0$ does indeed re-

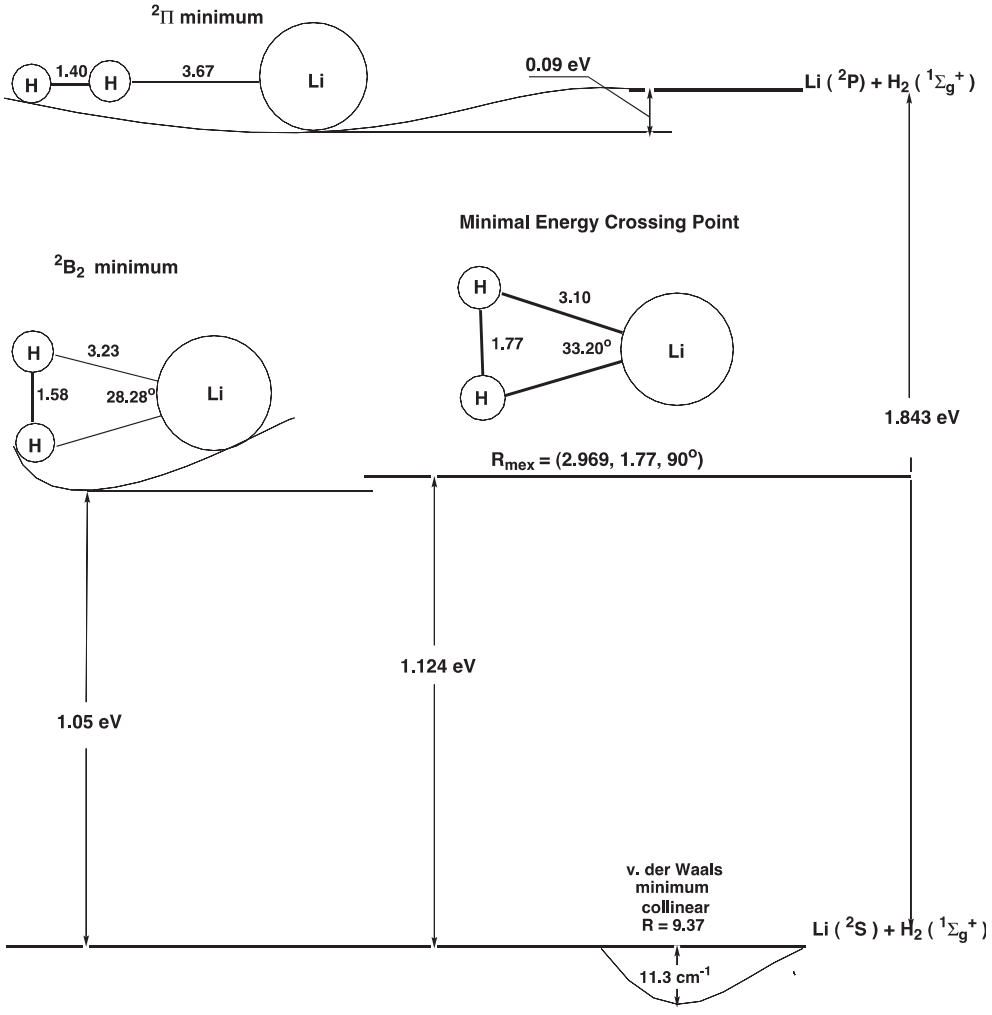

Fig. 1. Geometries and energies of extrema on the 1, $2^2A'$ and $1^2A''$ PESs of the Li + H_2 complex. The ground-state PES possesses a *van der Waals minimum* in a collinear configuration. The *1^2B_2 minimum* of the $2^2A'$ PES lies about 1.05 eV above the product asymptote. The *$^2\Pi$ minimum* of the $1^2A''$ PES is located only 0.09 eV below the reactant asymptote. The energy of the *minimal energy crossing point* is shown schematically

flect the existence of a trifurcation of the seam of conical intersection (see Fig. 3). Equivalently, the trifurcation represents a confluence of the C_{2v} seam with a seam of only C_s symmetry at $\mathbf{R}_{\text{tri}}$, where $\mathbf{R}_{\text{tri}} = \mathbf{R}_x(1.28) = (1.85, 1.28, 90°)$, and $E[\mathbf{R}_{\text{tri}}] \cong 6.0$ eV.

Although these trifurcations have now been located for several M–H_2 systems, including M = B [38], C [71], Al [36], and Cl^+[72] as well as ozone [35], this work represents the first report of this feature for an alkali metal atom and raises the question of its existence for other alkali metal–H_2 systems.

3.2.2 The C_s portion

Table 2 presents points on the C_s portion of the $1^2A' - 2^2A'$ seam of conical intersection, denoted $\mathbf{R}_x^{\text{Cs}}(\gamma) = (\mathbf{R}(\gamma), r(\gamma), \gamma)$ with the superscript Cs suppressed when no confusion results. To each point in Table 2 there corresponds a mirror image obtained by the replacement $\gamma \rightarrow 180° - \gamma$. $E[\mathbf{R}_x(87.577°)] = 6.227$ eV and $E[\mathbf{R}_x]$ increases, as does R(H-H), as γ deviates from 90° (Fig. 4). $||\mathbf{t}_{IJ}[\mathbf{R}_x(87.577°)]||$ is quite small as expected. However $||\mathbf{t}_{IJ}[\mathbf{R}_x(\gamma)]||$ remains small as γ increases. Comparing the energies plotted in Figs. 1 and 2, one concludes that the C_{2v} portion of the seam of conical intersection is absolutely preeminent in quenching reaction (1).

As noted in the Introduction Matsumoto and coworkers [10] reported an avoided crossing of the $1^2A'$ and $2^2A'$ states at $\gamma = 45°$. The seam point $\mathbf{R}_x(47.669°) = (1.872, 1.582, 47.669°)$ is very close to that point and $E[\mathbf{R}_x(47.669°)] = 8.08$ eV lies rather close to its calculated energy of ~8.36 eV [10]. Thus the avoided intersection is now seen to be a harbinger of the C_s portion of the seam of conical intersection.

The crossing point $\mathbf{R}_x(117.485°) = (1.806, 1.386, 117.485°)$ for $E[\mathbf{R}_x(117.485°)]$ ~6.82 eV is shown in Fig. 3. The existence of a trifurcation permits loops enclosing three points of conical intersection. A schematic of such a loop is also drawn in Fig. 3. Note that it is not necessary that these three crossing points lie in a common $\mathbf{g} - \mathbf{h}$ plane as shown.

3.3 Potential energy surfaces

Sections of the $1, 2^2A'$ PESs were considered in order to establish the energetics associated with reaching the conical intersection seam. In view of the range of r for which low-energy C_{2v} conical intersections exist, the

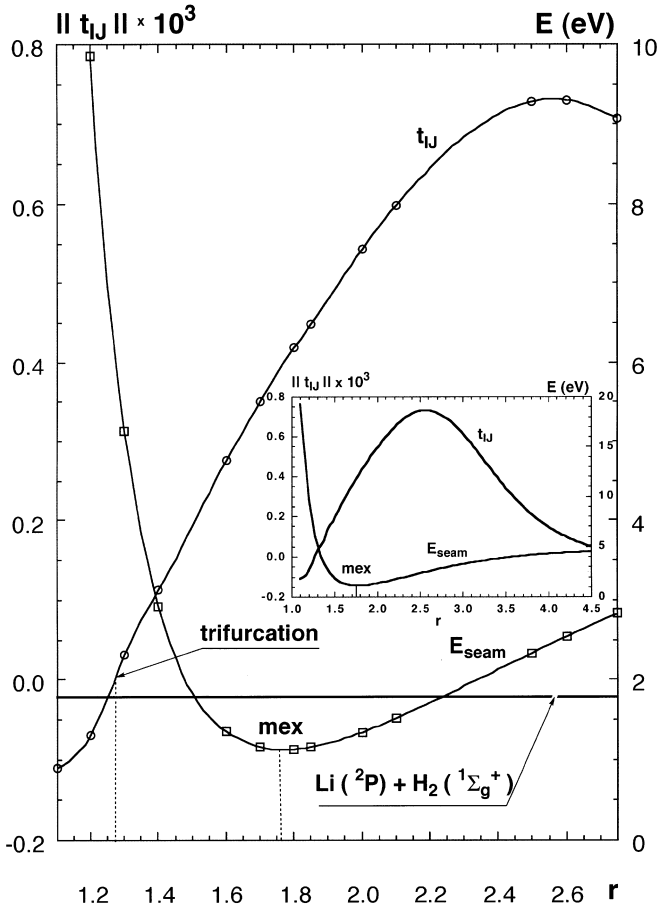

Fig. 2. Energy in eV relative to $E_{1^2A'}(\mathbf{R}_{\rm asym})$ and $\pm\|\mathbf{t}^{IJ}[\mathbf{R}_x(r)]\|$ multiplied by 10^3 on C_{2v} portion of seam as a function of seam parameter r (in bohr). See text

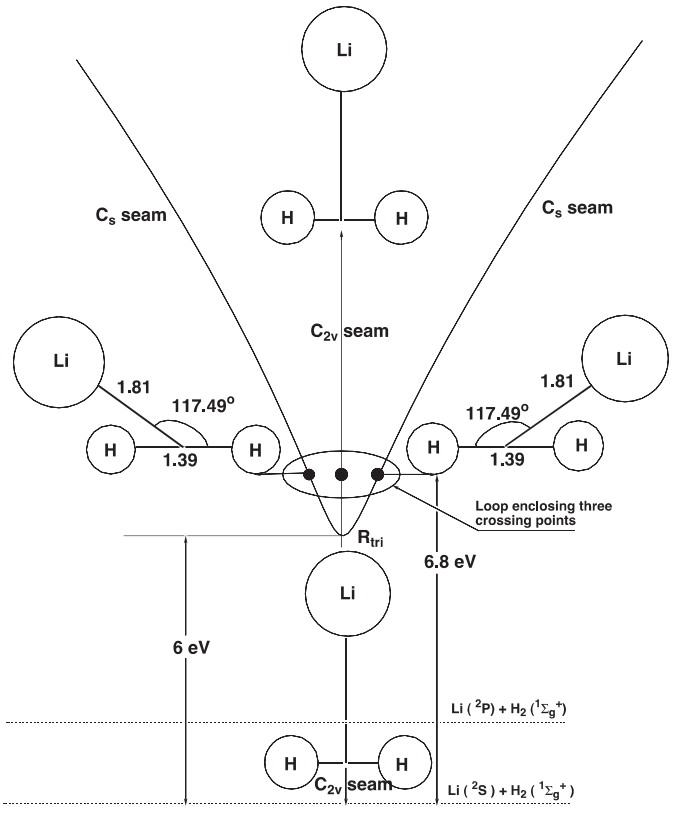

Fig. 3. $C_{2v} - C_s$ trifurcation of the seam of conical intersection

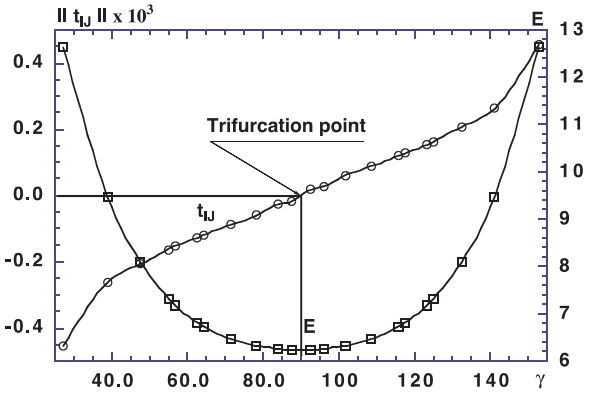

Fig. 4. Properties of the C_s seam. Energy in eV relative to $E_{1^2A'}(\mathbf{R}_{\rm asym})$; angle in degrees

$1^2A_1, 1^2B_2\, C_{2v}$ sections of the $1^2A', 2^2A'$ states, are displayed in Fig. 5 over the range $r = 1.0$, 1.5, 2.0, 2.5, 3.0, and $r = r_e(H_2) = 1.4011\, a_0$ and $R = 1 - 6\, a_0$.

In this range of R, the 1^2A_1 PES is repulsive. The 1^2B_2 PES is attractive with a global minimum at $\mathbf{R}_e^{B_2} = (3.136, 1.580, 90°)$. The H-H bond is diluted by approximately 0.18 a_0 in order to bind the Li atom. $\mathbf{R}_e^{B_2}$ is in good agreement with the previous results of Matsumoto and coworkers, $\mathbf{R}_e^{B_2} = (3.3, 1.5, 90°)$ [12], Hobza and Schleyer, $\mathbf{R}_e^{B_2} = (3.22, 1.52, 90°)$ [15], Boldyrev and Simons, $\mathbf{R}_e^{B_2} = (3.25, 1.54, 90°)$ [21], and Chaban and Gordon, $\mathbf{R}_e^{B_2} = (3.14, 1.58, 90°)$ [19]. $E_{2^2A'}(\mathbf{R}_e^{B_2}) = 1.05$ eV, that is about 0.8 eV below $E_{2^2A'}(\mathbf{R}_{\rm asym})$ (see Fig. 1), in good accord with 1.13 eV found by Hobza and Schleyer [15], 1.063 eV found by Boldyrev and Simons [21], and 1.054 eV reported by Chaban and Gordon [19]. No other minima were found on this PES.

Figure 5 evinces intersections of the 1^2A_1 and 1^2B_2 PESs at $\mathbf{R}_x(1.5) = (2.5, 1.5, 90°)$ with an energy $E[\mathbf{R}_x(1.5)] = 1.9$ eV, at $\mathbf{R}_x(2.0) = (3.4, 2.0, 90°)$ with $E[\mathbf{R}_x(2.0)] = 1.3$ eV, at $\mathbf{R}_x(2.5) = (4.3, 2.5, 90°)$ with $E[\mathbf{R}_x(2.5)] = 2.3$ eV, and, finally, at $\mathbf{R}_x(3.0) = (5.2, 3.0, 90°)$ with $E[\mathbf{R}_x(3.0)] = 3.3$ eV. These results are in excellent accord with those presented in Table 1 strongly supporting the compatibility of the treatments used herein.

We next turn to the $1^2\Sigma^+$ and $1^2\Pi$ $C_{\infty v}$ sections of the $1, 2^2A'$ PESs presented for $r = 1.0$, 1.4, 2.0, 2.5, and $3.0\, a_0$ and $R(\text{Li-H}^1) = 1 - 6\, a_0$ in Fig. 6. H^1 is defined as the closer H atom to Li. The energy difference between these states at $\mathbf{R}_{\rm asym}$ is 1.841 eV as expected from the magnitude of the excitation energy $\Delta E(^2S \rightarrow {}^2P)$ noted previously. The $1^2\Pi$ section of the $2^2A'$ PES is relatively flat with a global minimum at $\mathbf{R}_e^{2\Pi} = (3.673, 1.4, 0°)$ and $E(\mathbf{R}_e^{2\Pi}) = 1.762$ eV, that is about 0.09 eV below the reactant asymptote (see also Fig.1). However, it is seen that motion in this region should not lead to quenching

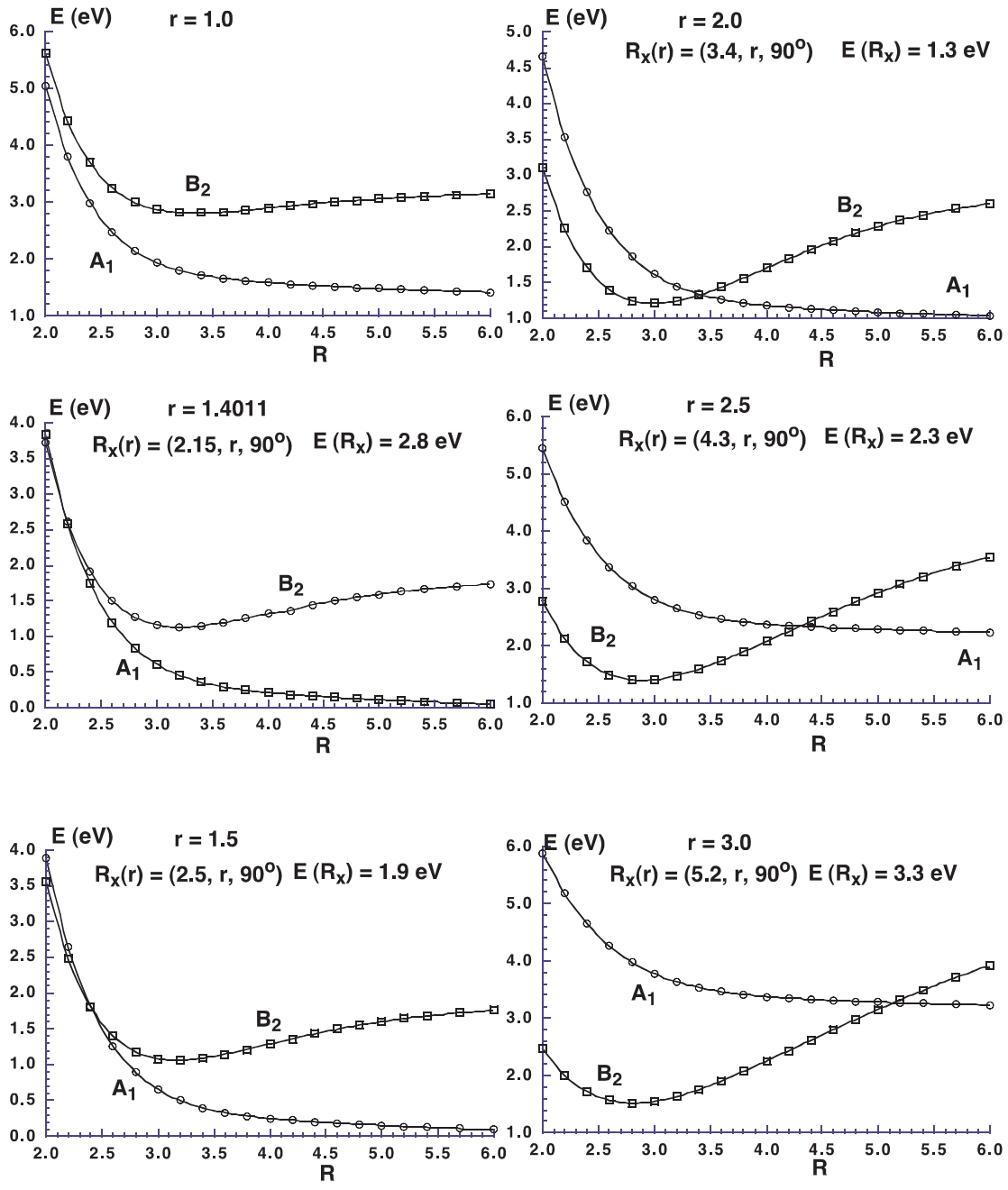

Fig. 5. Two lowest potential energy curves for T-shaped Li + H_2 complex with different H-H bond lengths. Energy in eV relative to $E_{1^2A'}(\mathbf{R}_{asym})$; distances in bohr

since there are no $^2\Sigma^+ - 1^2\Pi$ intersections over the range of geometries considered.

3.4 Implication for dynamics

Figure 2 shows the absence of a barrier to the seam of conical intersections. Thus the seam can be directly accessed from the reactant channel. It is worth noting, however, that $\mathbf{R}_e^{B_2} = (3.136, 1.580, 90°)$ with $E_{2^2A'}(\mathbf{R}_e^{B_2}) = 1.051$ eV, whereas $\mathbf{R}_{mex} = (2.969, 1.770, 90.0°)$ with the MECP energy $E_{2^2A'}(\mathbf{R}_{mex}) = 1.124$ eV. Thus the minimum energy path on the $2^2A'$ PES is expected to pass first through the exciplex on the $2^2A'$ PES where the separation between the $E_{2^2A'}$ and $E_{1^2A'}$ states is approximately 0.4 eV.

The seam point which is (geometrically) closest to $\mathbf{R}_e^{B_2}$ is $\mathbf{R}_x(1.84) = (3.106, 1.84, 90°)$ with $E_{2^2A'}(\mathbf{R}_x(1.84)) - E_{2^2A'}(\mathbf{R}_e^{B_2})$ being only 0.095 eV. Therefore, it can be anticipated that the formation of the exciplex may favor nonadiabatic transitions in the region of the crossing point $\mathbf{R}_x(1.84)$. Further deviations from the minimum energy path can lead to nonadiabatic transitions over the range of conical intersection points on the energetically accessible portion of the seam. It would be interesting to use trajectory surface hopping techniques to address this issue [29].

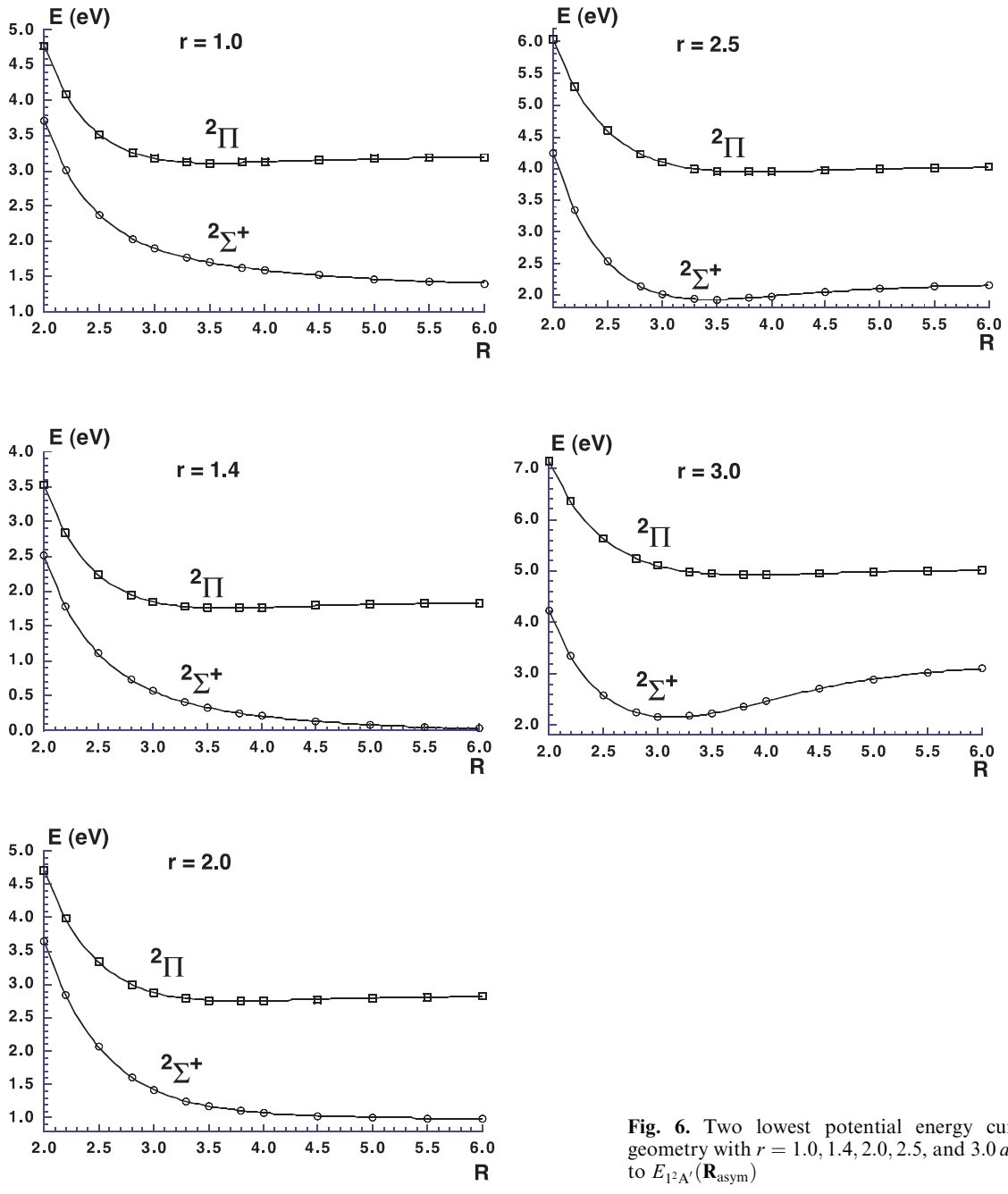

Fig. 6. Two lowest potential energy curves for the collinear geometry with $r = 1.0, 1.4, 2.0, 2.5$, and $3.0\,a_0$. Energy in eV relative to $E_{1^2A'}(\mathbf{R}_{\text{asym}})$

A qualitative model of the relation between the crossing point and the ro-vibrational excitation of the H_2 molecule is provided by the bond-dilution model (see Refs. [28, 69] and references therein). Applying this model and the ro-vibrational data for H_2 [73], it is found that the nonadiabatic transition at the crossing point $\mathbf{R}_x(2.0)$ causes vibrational-rotational excitation of H_2 to $v \leq 1$ and $J \leq 5$, whereas a transition at $\mathbf{R}_x(2.1)$ allows higher rotational excitations to $J \leq 8$. Further dilution of the H-H bond, for instance, at the crossing point $\mathbf{R}_x(2.57)$, promotes the vibrational excitation of the H_2 molecule to a higher quantum number, $v \leq 4$, and simultaneously diminishes its rotational quantum number to $J \leq 6$. Interestingly, $\mathbf{R}_{\text{mex}}$ allows only rotational excitation of the quenching H_2 molecule to $J \leq 5$.

3.5 Analyzing the seam of conical intersection

The energetics, derivative couplings, and the nature of the diabatic states in the vicinity of the seam of conical intersection are the key to understanding reaction (1). The perturbation theory outlined in Sec. 2 can provide a valuable tool for characterizing this region, obviating the need for detailed ab initio calculations. Therefore, we study the performance of perturbation theory and

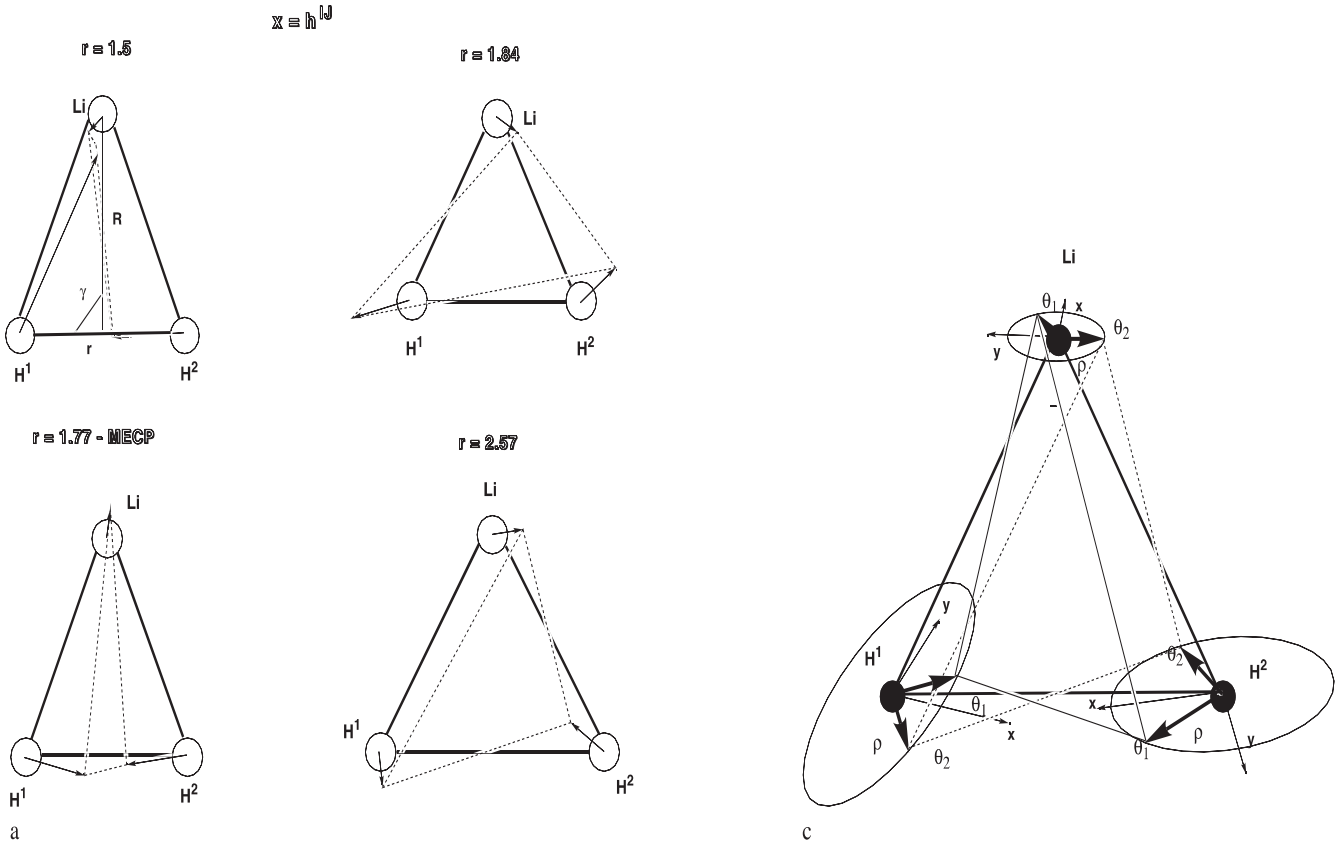

Fig. 7a–c. $\mathbf{g} - \mathbf{h}(\mathbf{R}_x)$ plane at representative points on C_{2v} seam. **a** The *x*- and **b** the *y*-axes of this plane are connected by a *dotted line*. **c** Two pictures of loop geometries corresponding to angles θ_1 and θ_2

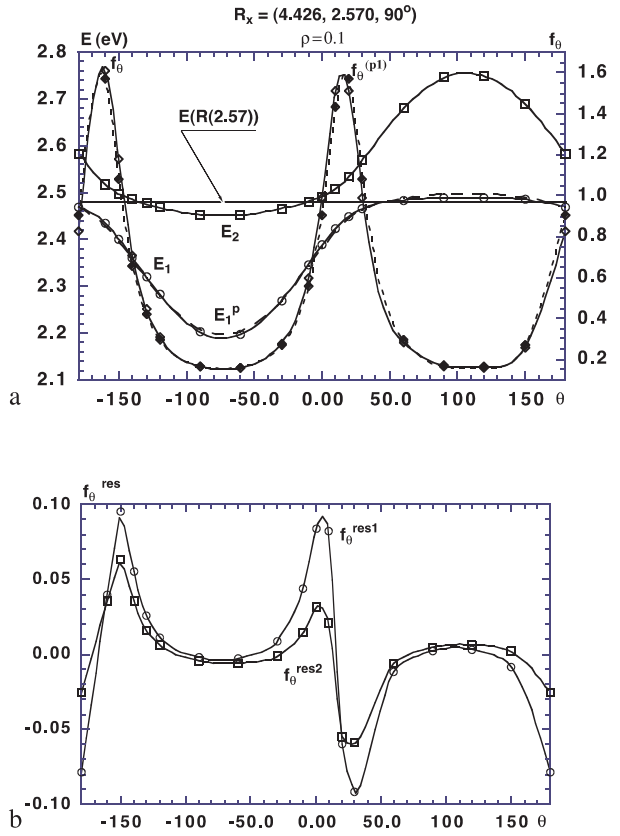

Fig. 8a, b. Results of the loop enclosing $\mathbf{R}_x(2.57)$ with $\rho = 0.1\,a_0$. **a** The energy $E_{1^2A'} = E_{I_\rho}$ is shown by *open circles*, the first-order perturbation energy $E^{(\mathrm{p1})}_{1^2A'} = E^p_I$ by a *long dashed line*, $E_{2^2A'} = E_2$ by *open squares*, f_θ by *open diamonds*, and $f^{(\mathrm{p1})}_\theta$ by a *short dashed line* with *filled diamonds*. Energies are taken with respect to $E_{1^2A'}(\mathbf{R}_{\mathrm{asym}})$. **b** Residual derivative couplings: $f^{\mathrm{res}i}_\theta = f_\theta - f^{(\mathrm{p}i)}_\theta, i = 1$ (*open circles*), 2 (*open squares*)

subsequently consider the nature of the diabatic states in the vicinity of the seam of conical intersection.

3.5.1 Characteristic parameters and the $\mathbf{g} - \mathbf{h}$ plane

In the immediate vicinity of a point of conical intersection the energy, $E^{(\mathrm{p1})}_I(\mathbf{R})$, the largest and singular part of the derivative coupling $(1/\rho)f_\theta$, and the electronic dipole moment may be expressed in terms of the characteristic parameters, $\mathbf{g}^{IJ}, \mathbf{h}^{IJ}$, and $\mathbf{s}^{IJ}$ as well as the dipole moment matrix at the conical intersection, $\boldsymbol{\mu}_{KL}(\mathbf{R}_x)(K, L = I, J)$. In this analysis, the $\mathbf{g} - \mathbf{h}(\mathbf{R})_x$ plane is a key tool since it guarantees that the derivative coupling attributable to internal coordinates perpendicular to that plane is nonsingular at the point of conical intersection in question. Hereafter we suppress the superscript IJ in the nonadiabatic derivative coupling.

Figure 7a and b portrays the vectors defining the $\mathbf{g} - \mathbf{h}(\mathbf{R}_x)$ plane at $\mathbf{R}_x$ in terms of nuclear displacements, $\mathbf{h}^{IJ}$ and $\mathbf{g}^{IJ\perp}$. From this figures it is seen that for $\mathbf{R}_{\mathrm{mex}}$, the vector $\mathbf{h}^{IJ}$ is largely C_{2v} preserving, describing mainly H-H stretch and R elongation, whereas $\mathbf{g}^{IJ\perp}$ is primarily responsible for C_{2v} symmetry breaking. However, in general, $\mathbf{h}^{IJ}$ does not retain C_{2v} symmetry. This is clearly

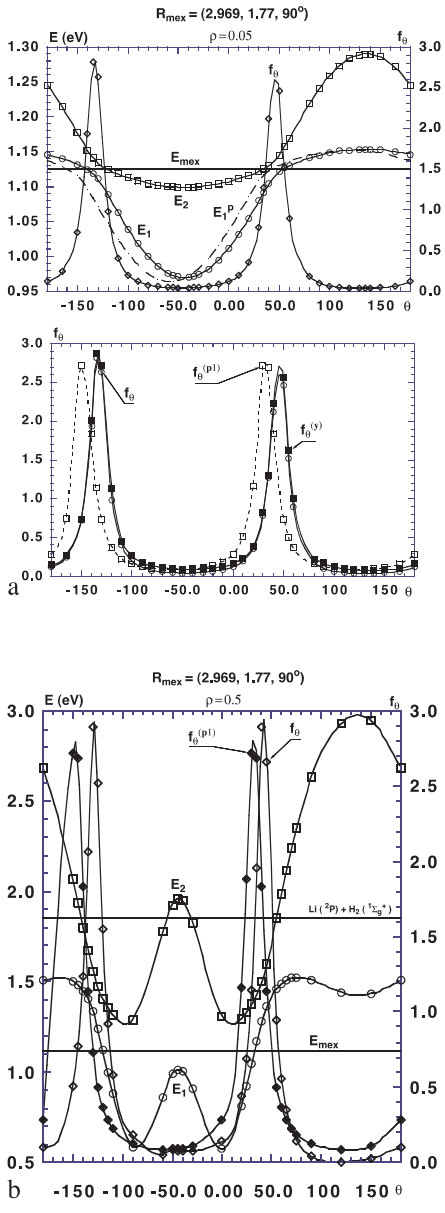

Fig. 9a, b. Energies and f_θ in local neighborhood of $\mathbf{R}_{\mathrm{mex}}$ for loops with **a** $\rho = 0.05\,a_0$ and **b** $0.5\,a_0$. Energies are taken with respect to $E_{1^2A'}(\mathbf{R}_{\mathrm{asym}})$. See caption to Fig. 8. For definition of $f^{(\mathrm{y})}_\theta$ see sect. 3.6

seen from $\mathbf{h}^{IJ}$ and $\mathbf{g}^{IJ\perp}$ at $\mathbf{R}_x(1.84)$ which both break C_{2v} symmetry. This does not reflect a "broken symmetry" wave function. Rather it is a consequence of the degeneracy at the conical intersection which permits a two-dimensional rotation of the states in question. Any symmetry breaking is evident in the vector $\mathbf{t}^{IJ}[\mathbf{R}_x]$ which, as noted previously, is invariant to this mixing.

In this work, all calculations in the vicinity of the C_{2v} conical intersection seam were, of necessity, performed within C_s symmetry. These calculations recover the C_{2v} symmetry of the C_{2v} portion of the seam to an excellent approximation. The minimal symmetry breaking which does occur has, however, no consequence on the results reported in this work. In particular, symmetry breaking cannot be responsible for the trifurcation reported here

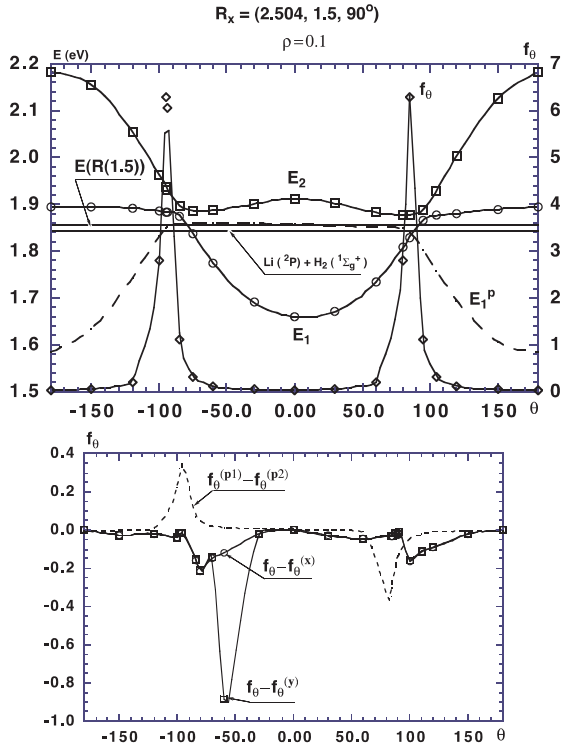

Fig. 10. Results of the loop enclosing $\mathbf{R}_x(1.5)$ with $\rho = 0.1\,a_0$. See caption to Fig. 8. In the *bottom panel*, the residual nonadiabatic derivative coupling is given by $f_\theta^{\mathrm{res}(w)} = f_\theta - f_\theta^{(w)} (w = x, y)$

since both C_{2v} and C_s points of conical intersection exist for $r > 1.28\,a_0$.

3.5.2 Loop analysis

For each $\mathbf{R}_x$ we use the polar coordinate system defined is Sect. 2.3. A closed loop of radius ρ in the $g - h$ plane, $C_\rho[\mathbf{R}_x(r)]$ surrounding $\mathbf{R}_x(r)$ is obtained by varying θ from $-180°$ to $+180°$ for fixed ρ and corresponds to a sequence of nuclear configurations. Such a sequence of configurations is shown schematically in Fig. 7c for $\mathbf{R}_x = \mathbf{R}_{\mathrm{mex}}$, where the α^{th} atom possesses its own $\mathbf{g} - \mathbf{h}_\alpha(\mathbf{R}_x)$ plane formed by $\mathbf{g}_\alpha^{IJ\perp}$ and $\mathbf{h}_\alpha^{IJ}$ given by Eqs. (16a) and (16b). The associated circle C_ρ^α in this $\mathbf{g} - \mathbf{h}_\alpha(\mathbf{R}_x)$ plane is also drawn. Rotating each atom along its own circle C_ρ^α in a concerted manner results in the loop $C_\rho[\mathbf{R}_x]$. The nuclear configurations of LiH_2 in the neighborhood of the MECP corresponding to two values of $\theta = \theta_1$ and $\theta = \theta_2$ are shown by solid and dashed lines in Fig. 7c.

The loop technique is a valuable tool for investigating the energetic and geometric neighborhood of the seam. The circulation of $\mathbf{f}^{IJ}$ along a loop of radius ρ centered at $\mathbf{R}_x$ defined as

$$X[C_\rho(\mathbf{R})] \equiv \oint_{C_\rho(\mathbf{R}_x)} \mathbf{f}^{IJ}(\mathbf{R}) \cdot d\mathbf{R} \tag{22}$$

has the following remarkable property: as $\rho \to 0$, $X[C_\rho(\mathbf{R})] \to \pi$ if $\mathbf{R}$ is a point of conical intersection, and is zero otherwise [39].

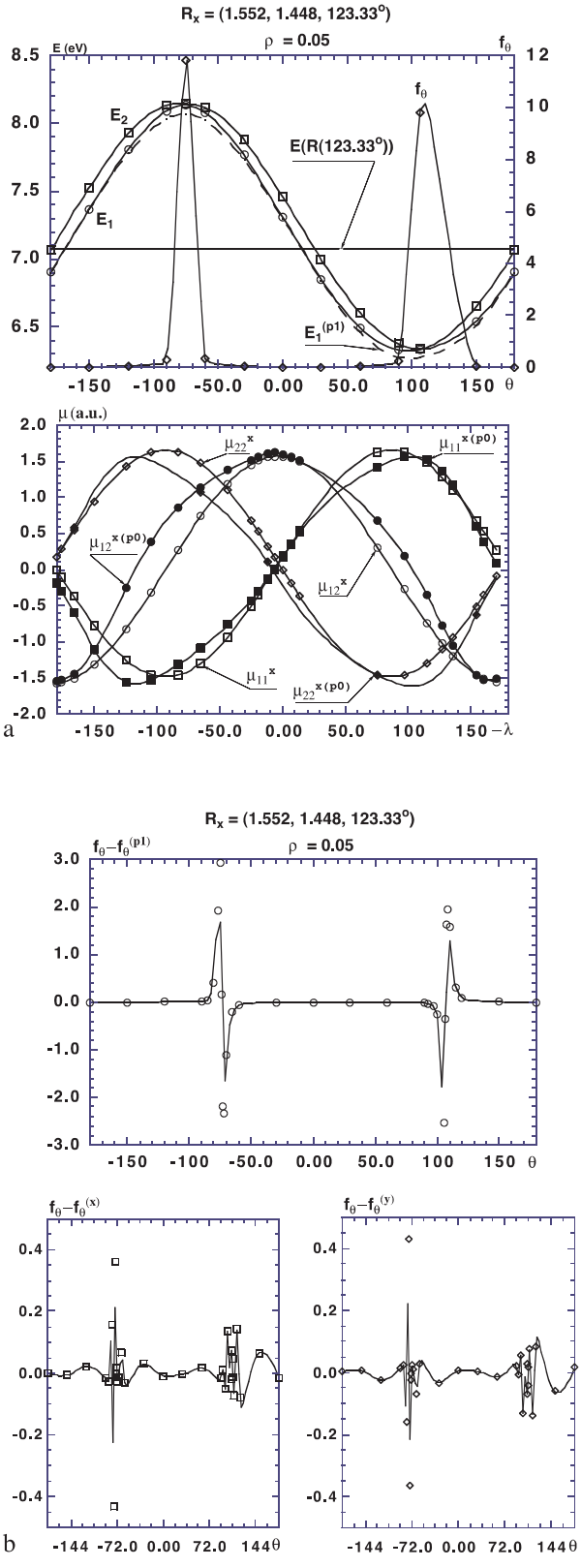

Fig. 11a, b. Loop $C_{0.05}$ around $\mathbf{R}_x(123.330°) = (1.552, 1.448, 123.330°)$. **a** Energies $E_{1^2A'}$ and $E_{2^2A'}$ are shown with respect to $E_{1^2A'}(\mathbf{R}_{\mathrm{asym}})$ together with f_θ (*open diamonds*). In the *bottom panel* the xth components of the dipole moments as functions of the angle λ are shown. **b** The residual nonadiabatic derivative couplings $f_\theta^{\mathrm{res1}} = f_\theta - f_\theta^{(\mathrm{p1})}$ (*open circles*) and $f_\theta^{\mathrm{res}(w)} = f_\theta - f_\theta^{(w)}$ [w = x (*open squares*), *y* (*open diamonds*)]

3.5.3 Energies, derivative couplings, and dipole moments near $\mathbf{R}_x$

We now analyze the captioned properties along $C_\rho(\mathbf{R}_x)$ in the $\mathbf{g}-\mathbf{h}(\mathbf{R}_x)$ plane. Here we focus on the vicinity of the crossing points $\mathbf{R}_x^{C2v}(2.57), \mathbf{R}_x^{C2v}(1.77) = \mathbf{R}_{mex}$, $\mathbf{R}_x^{C2v}(1.5)$, and $\mathbf{R}_x^{Cs}(123.33°)$, ordered in decreasing magnitude of $||\mathbf{t}^{IJ}[\mathbf{R}_x]||$ although the analysis may be repeated for any point of conical intersection using the characteristic parameters given in Tables 1 and 2. It is anticipated, and will be demonstrated below, that for a given ρ, the reliability of the perturbation treatment will increase with $||\mathbf{t}^{IJ}[\mathbf{R}_x(r)]||$. It is useful to note that $X[C_\rho(\mathbf{R}_x)]/\pi$ is approximately 1.00 along all loops examined in this section, demonstrating that each loop in fact contains a point of conical intersection.

For $\mathbf{R}_x(2.57) = (4.43, 2.57, 90°)$ consider the loop $C_{0.1}[\mathbf{R}_x(2.57)]$. $E_{1^2A'}$ and $E_{2^2A'}$, and the first-order perturbation energy $E_{1^2A}^{(p1)}$ are plotted in Fig. 8a. $E_{2^2A'}$ is above $E_{2^2A'}(\mathbf{R}_{asym})$ for all points on this loop so this region is only accessible for molecules with appreciable internal energy. The key point here is the good agreement between the perturbative treatment and the explicit computational results. Two avoided crossings at $\theta = -160°$ and $20°$ with an energy gap $[E_{2^2A'} - E_{1^2A'}] = 0.082$ eV are observed. The corresponding structures in Jacobi coordinates are $\mathbf{R}_x[\rho = 0.1,\ \theta = -160°; \mathbf{R}_x(2.57)] = (4.43, 2.57, 86.47°)$ and $\mathbf{R}_x[\rho = 0.1,\ \theta = 20°;\ \mathbf{R}_x(2.57)] = (4.42, 2.58, 93.51°)$ respectively. Note that the corresponding γ sum to about 180°. The slight differences in R and r for these points evince a small symmetry breaking. This small symmetry breaking was anticipated on the basis of a small component in the y-direction of $\mathbf{t}^{IJ}[\mathbf{R}_x\ (2.57)]$. The derivative couplings f_θ and $f_\theta^{(p1)}$ are also shown in Fig. 8a. Figure 8b shows the ith residual derivative coupling $f_\theta^{resi} = f_\theta - f_\theta^{(pi)}$, where $i = 1$ and 2 for the first-order perturbation treatment and a second-order perturbation treatment reported elsewhere [61]. From Fig. 8b, one concludes that the first-order perturbation treatment covers about 90% of the calculated derivative coupling and the second order improves it to 97%.

We next turn to an analysis of a neighborhood of the MECP $\mathbf{R}_{mex} = \mathbf{R}_x(1.77)$. Figure 9 depicts the results for $C_\rho[\mathbf{R}_{mex}]$ with $\rho = 0.05$ and $0.5\,a_0$. Note that for $\rho = 0.05$, the results of the perturbative treatment and the actual calculations agree less well than those for $\mathbf{R}_x(2.57)$. With regard to the derivative coupling, as seen in the bottom panel of Fig. 9a, a shift by about 10° between the peaks of f_θ and its first-order perturbation estimate $f_\theta^{(p1)}$ is clearly evident. The reason for this can be inferred from Fig. 2, where it is seen that $||\mathbf{t}^{IJ}[\mathbf{R}_x]||$ decreases by 45% in going from $\mathbf{R}_x(2.57)$ to $\mathbf{R}_x(1.77)$. This indicates that the size of the first-order terms has diminished and second-order effects, not included in the perturbative expression for the energy, play an increased role.

The smaller loop $C_{0.05}[\mathbf{R}_{mex}]$ yields two structures $\mathbf{R}_x$ $(\rho = 0.05,\ \theta \cong -1.35°;\ \mathbf{R}_{mex}) = (2.968,\ 1.772,\ 87.43°)$ and $\mathbf{R}_x(\rho = 0.05,\ \theta \cong 50°; \mathbf{R}_{mex}) = (2.968, 1.775, 92.57°)$ with rather small energy gaps ($\sim$0.023 eV) and large f_θ (see bottom panel in Fig. 9a). Note that $E_{2^2A'}(\mathbf{R})$ for any $\mathbf{R}$ covered by $C_{0.05}[\mathbf{R}_{mex}]$ with $-160° \le \theta \le 70°$ lies below $E_{2^2A'}(\mathbf{R}_{asym})$.

The results for the larger loop $C_{0.5}[\mathbf{R}_{mex}]$ shown in Fig. 9b differ significantly from those of $C_{0.05}[\mathbf{R}_{mex}]$. Again two avoided crossing are identified at $\mathbf{R}_x(\rho = 0.5, \theta \cong -1.30°; \mathbf{R}_{mex}) = (3.00, 1.84, 64.70°)$ and $\mathbf{R}_x(\rho = 0.5, \theta \cong 40°;\ \mathbf{R}_{mex}) = (3.01,\ 1.81,\ 115.51°)$. However, here for each state there is a barrier with the nearly T-shaped nuclear structure $\mathbf{R}_x(\rho = 0.5, \theta \cong -43°; \mathbf{R}_{mex}) = (3.21, 1.12, 89.01°)$ reflecting a significantly compressed H-H bond. These barriers in turn separate minima symmetrically disposed about the approximate C_{2v} maximum at $\theta \cong -90°$ and 0° corresponding to $\mathbf{R}_x(\rho = 0.5,\ \theta \cong -90°;\ \mathbf{R}_{mex}) = (3.14, 1.40,\ 67.27°)$ and $\mathbf{R}_x(\rho = 0.5,\ \theta \cong 0°;\ \mathbf{R}_{mex}) = (3.15,\ 1.37,\ 111.90°)$. For much of this loop $E_{2^2A'}$ lies above $E_{2^2A'}(\mathbf{R}_{asym})$.

The crossing point $\mathbf{R}_x(1.5)$, which energetically is very close to the reactant asymptote, is considered next. Figure 10 shows the results for $C_{0.1}[\mathbf{R}_x(1.5)]$. In this case $E_{2^2A'}$ is uniformly endoergic relative to $E_{2^2A'}$. It is seen that the computed energy and perturbative result differ significantly. Also, as shown in the bottom panel of Fig. 10, the first-order derivative coupling $f_\theta^{(p1)}$ is shifted from f_θ, as in Fig. 9a for the MECP. The second-order derivative $f_\theta^{(p2)}$ does not cure this discrepancy. $f_\theta^{(p2)} - f_\theta^{(p1)}$ is shown by a dashed line in the bottom panel of Fig. 10. These differences reflect the factor of 2 decrease in $||\mathbf{t}^{IJ}[\mathbf{R}_x]||$ in going from $\mathbf{R}_x(1.77)$ to $\mathbf{R}_x(1.5)$. Looking at the behavior of f_θ reveals the existence of two avoided crossing points at $\theta = \pm 90°$ almost symmetrically located with respect to $\theta = 0°$ and corresponding to the slightly C_{2v} distorted structures $\mathbf{R}_x[\rho = 0.1,\ \theta = -90°;\ \mathbf{R}_x(1.5)] = (2.39, 1.52, 83.91°)$ and $\mathbf{R}_x[\rho = 0.1,\ \theta = 90°;\ \mathbf{R}_x(1.5)] = (2.40,\ 1.49,\ 96.15°)$. The point $\mathbf{R}_x[\rho = 0.1,\ \theta = 0°;\ \mathbf{R}_x(1.5)] = (2.43, 1.37, 89.45°)$ is characterized by the energy gap $E_{2^2A'} - E_{1^2A'} = 0.25$ eV.

Finally we consider the point $\mathbf{R}_x^{Cs}(123.33°) = (1.827,\ 1.448,\ 123.33°)$ using $C_{0.05}[\mathbf{R}_x(123.33°)]$. The corresponding energy profile is shown in Fig. 11a. The energetics along this loop differs markedly from those reported previously. The curves appear almost parallel although avoided crossings near $\mathbf{R}_x[\rho = 0.05,\ \theta = -75°;\ \mathbf{R}_x(123.33°)] = (1.770,\ 1.446,\ 55.57°)$ and $\mathbf{R}_x[\rho = 0.05,\ \theta = 107°;\ \mathbf{R}_x(123.33°)] = (1.884,\ 1.452,\ 57.79°)$ are evident from the sharply peaked derivative couplings. This behavior reflects the increased importance of $\mathbf{s}^{IJ}(\mathbf{R}_x)$ for the C_s conical intersection points when compared with the C_{2v} points (see also Tables 1 and 2).

f_θ^{res1} is reported in the upper panel of Fig. 11b. From this data one recognizes that the peaks of $f_\theta^{(p1)}$ are slightly shifted from those of f_θ as above. These differences are not unexpected in view of the relatively small value of $\|\mathbf{t}^{IJ}[\mathbf{R}_x(123.33°)]\|$. Fig. 11a also shows the dependence of the dipole moments $\boldsymbol{\mu}_{II}$ and $\boldsymbol{\mu}_{JJ}$, and the transition dipole moment $\boldsymbol{\mu}_{IJ}$ as functions of the angle λ defined by Eq. (19). It is clear that the λ-dependence of these dipole moments has a simple oscillatory form (see Eq. 22). This differs markedly from the dependence of these quantities on θ which exhibits the abrupt changes characteristic of an avoided crossing. Finally note that

$\boldsymbol{\mu}_{KL}$ and $\boldsymbol{\mu}_{KL}^{(\mathrm{p0})}$ are in only qualitative agreement. This again reflects the small value of $\|\mathbf{t}^{IJ}[\mathbf{R}_x(123.33^\circ)]\|$, since improved agreement between $\boldsymbol{\mu}_{KL}$ and $\boldsymbol{\mu}_{KL}^{(\mathrm{p0})}$ is observed as $\|\mathbf{t}^{IJ}[\mathbf{R}_x]\|$ increases.

3.6 Determination of the adiabatic-to-diabatic mixing angle

In this section we consider the performance of the adiabatic-diabatic state transformation, suggested by Werner and Meyer, in the vicinity of the conical intersection. In particular, f_θ determined from the ab initio wave functions is compared with that deduced from the Werner-Meyer transformation and from perturbation theory. This study uses $C_{0.05}[\mathbf{R}_x^{\mathrm{C2v}}(1.77)]$, $C_{0.1}[\mathbf{R}_x^{\mathrm{C2v}}(1.5)]$, and $C_{0.05}[\mathbf{R}_x^{\mathrm{Cs}}(123.33^\circ)]$. In the bottom panel of Fig. 9a we demonstrate the dependence of f_θ, $f_\theta^{(\mathrm{p1})}$, and $f_\theta^{(y)} = \frac{\partial}{\partial\theta}\beta^{\mu^y}_{\kappa=0}$ as functions of the loop angle θ around the MECP. Here $\beta^{\mu^y}_{\kappa=0}$ is obtained from Eq. (14a) with $A = \mu^w$. It is seen that $f_\theta^{(y)}$ essentially reproduces f_θ in the whole range of the loop angle and is generally superior to $f_\theta^{(\mathrm{p1})}$. In particular, at the peaks of f_θ the relative error comprises $\leq 5\%$.

In Fig. 10 we plot the residual derivative couplings $f_\theta^{\mathrm{res}(w)} = f_\theta - f_\theta^{(w)}$ ($w = x$ or y) for $C_{0.1}[\mathbf{R}_x(1.5)]$. $f_\theta^{\mathrm{res}(x)}$ slightly deviates from zero in the neighborhood of the peaks of f_θ with the maximum deviation comprising about 3% of the peak magnitude. $f_\theta^{(x)}$ produces better results than the second-order perturbative treatment, a not unexpected result in view of the size of $\|\mathbf{t}^{IJ}[\mathbf{R}_x(1.5)]\|$. On the other hand, although $f_\theta^{(y)}$ reproduces f_θ quite well, $f_\theta^{\mathrm{res}(y)}$ at $\theta = -60^\circ$ is about 12% of the actual value of f_θ and is about 4 times larger than $f_\theta^{\mathrm{res}(x)}$.

The residual derivative coupling f_θ^{res1} is compared with $f_\theta^{\mathrm{res}(x)}$ and $f_\theta^{\mathrm{res}(y)}$ for $C_{0.05}[\mathbf{R}_x^{\mathrm{Cs}}(123.33^\circ)]$ in Fig. 11b. Inspecting this figure, one arrives at the conclusion that the derivative couplings obtained by means of the Werner-Meyer formula rather accurately describe the calculated derivative coupling and in this case, where $\|\mathbf{t}^{IJ}[\mathbf{R}_x^{\mathrm{Cs}}(123.33^\circ)]\|$ is small, are superior to the first-order perturbation estimate.

4 Summary and conclusions

The focus of the present work is the nonreactive nonadiabatic quenching reaction $\mathrm{Li}(1s^2 2p;\, ^2\mathrm{P}) + \mathrm{H}_2(^1\Sigma_g^+) \rightarrow \mathrm{LiH}_2(2^2\mathrm{A}') \rightarrow \mathrm{LiH}_2(1^2\mathrm{A}') \rightarrow \mathrm{Li}\ (1s^2 2s;\, ^2\mathrm{S}) + \mathrm{H}_2(^1\Sigma_g^+)$. The nonadiabatic transition $\mathrm{LiH}_2(2^2\mathrm{A}') \rightarrow \mathrm{LiH}_2(1^2\mathrm{A}')$ is facilitated by a symmetry-allowed $^2\mathrm{B}_2 - {}^2\mathrm{A}_1$ seam of conical intersection. The $^2\mathrm{B}_2$ section of the $2^2\mathrm{A}'$ state has a bound exciplex at $\mathbf{R}_e^{\mathrm{B}_2} = (3.136,\ 1.580,\ 90^\circ)$ with an energy $E_{2^2\mathrm{A}'}(\mathbf{R}_e^{\mathrm{B}_2})$ lying 0.8 eV below the $\mathrm{Li}(^2\mathrm{P}) + \mathrm{H}_2$ asymptote. The point of closest approach to the exciplex on the seam of conical intersection is $\mathbf{R}_x(1.84) = (3.106,\ 1.837,\ 90^\circ)$ with $E_{2^2\mathrm{A}'}(\mathbf{R}_x(1.84)) - E_{2^2\mathrm{A}'}(\mathbf{R}_e^{\mathrm{B}_2})$ only 0.095 eV. The exciplex neighborhood also includes the MECP $\mathbf{R}_{\mathrm{mex}} = (2.969,\ 1.770,\ 90.0^\circ)$, for which $E_{2^2\mathrm{A}'}(\mathbf{R}_x(1.77)) - E_{2^2\mathrm{A}'}(\mathbf{R}_e^{\mathrm{B}_2}) = 0.073$ eV.

The C_{2v} seam of conical intersection is carefully studied. For each point on the C_{2v} seam, the $\mathbf{g} - \mathbf{h}$ plane and the tangent vector, $\mathbf{t}^{IJ} \equiv \mathbf{g}^{IJ} \times \mathbf{h}^{IJ}$ are reported. Determination of the $\mathbf{g} - \mathbf{h}$ plane is the key to the analysis of a point of conical intersection since this plane contains the entire linear or conical part of the intersecting surfaces. Using the vanishing of $\mathbf{t}^{IJ}$ as a criterion for trifurcation, we are able to show the $1^2\mathrm{A}' - 2^2\mathrm{A}'$ seam actually consists of two portions: the $C_{2v}\ ^2\mathrm{B}_2 - {}^2\mathrm{A}_1$ symmetry-allowed portion noted above and the C_s portion that intersects the C_{2v} portion near $\mathbf{R}_x(1.28) = (1.8,\ 1.28,\ 90^\circ)$, with $E_{2^2\mathrm{A}'}(\mathbf{R}_x(1.28)) \cong 6.0$ eV. This trifurcation of the C_{2v} seam occurs at energies too high to influence the dynamics of the quenching process. In future work it will be interesting to see whether this feature occurs in other alkali metal–H_2 systems.

Energies, derivative couplings, and dipole matrix elements are determined for closed loops in the $\mathbf{g} - \mathbf{h}$ plane for points on both the C_s and C_{2v} portions of the seam of conical intersection. This provides a vivid picture of the energetics and derivative coupling patterns in the local neighborhood of the seam. The loop technique inspires us to study possible ways to determine the adiabatic-to-diabatic mixing angle by means of some electronic properties and, speaking generally, also to investigate some properties of nonadiabatic derivative coupling. We demonstrate that the derivative coupling obtained by differentiating the Werner-Meyer mixing angle describes rather accurately the (ultimately) singular part of the derivative coupling near a conical intersection.

We also calculate sections of the PESs involved in quenching reaction (1). For collinear geometries we find that the $^2\Sigma^+$ PES becomes attractive at fixed $r \geq 2.42\, a_0$, while the lowest $^2\Pi$ PES is always attractive, at least for H-H separations $\geq 1.0\, a_0$, and thus, possesses the global minimum with $R(\mathrm{Li\text{-}H}^1) = 3.673$ and $r = 1.400\, a_0$. It is located just 0.09 eV below the reactant asymptote. These $^2\Sigma^+$ and $^2\Pi$ states do not intersect in the range of r studied. We also locate a van der Waals-like saddle point on the ground-state PES for the perpendicular configuration $\mathbf{R}_{\mathrm{vts}} = (10.66,\ 1.4011,\ 90^\circ)$ with an energy of 5.6 cm^{-1} and a van der Waals minimum for the collinear configuration with $\mathbf{R}_{\mathrm{vm}} = (9.37,\ 1.4011,\ 0^\circ)$ characterized by a well depth of 11.3 cm^{-1}.

Acknowledgements. The authors thank Prof. Peter Botschwina for his invitation to contribute to the Special Issue of Theoretical Chemical Accounts in honor of Prof. Wilfried Meyer. Professor Morris Krauss is acknowledged for providing us with a reprint of his paper. One of the authors, E.S.K., thanks Dr. Nikita Matsunaga for his invaluable help with some computational programs, Dr. Galina Chaban for useful discussions, and Prof. Lorenz Cederbaum and Prof. Antonio Macías for enlightening discussions and warm hospitality. The calculations reported in this work were performed on D.R.Y's IBM RS 6000 workstations purchased with funds provided by AFOSR, NSF and, DOE-BES. E.S.K. is supported part DOE-BES grant DE-FE02-91ER14189. D.R.Y. is supported by AFOSR grant F49620-96-1-0017.

Appendix

Table 1. C_{2v} portion of seam of conical intersection of Li + H_2 in Cartesian coordinates

Atom	x	y	h_x^{IJ}	h_y^{IJ}	g_x^{IJ}	g_y^{IJ}
	$r = 1.1$	$R = 1.226$	$E = 19.302$	$\|\mathbf{t}^{IJ}\|$	$= -0.00011$	
Li	0.0000	1.3577	0.0216	1.5741	−0.7308	1.4915
H	0.5504	0.1312	−0.1419	0.0325	0.9262	−0.2288
H	−0.5496	0.1329	0.1211	0.0152	−0.1945	0.3591
	$s_x = 0.0713$	$s_y = -0.2794$	$s_z = -1.7265$			
	$r = 1.2$	$R = 1.547$	$E = 9.852$	$\|\mathbf{t}^{IJ}\|$	$= -0.00007$	
Li	0.0000	1.3577	0.0097	1.5760	−0.4962	1.3324
H	0.6004	−0.1899	−0.0857	−0.2916	0.8310	−0.7381
H	−0.5996	−0.1883	0.0768	−0.3048	−0.3341	0.3853
	$s_x = 0.0086$	$s_y = 0.0336$	$s_z = -0.8945$			
	$r = 1.3$	$R = 1.8597$	$E = 5.134$	$\|\mathbf{t}^{IJ}\|$	$= 0.00003$	
Li	0.0000	1.3577	−0.0015	1.1282	0.2740	1.3364
H	0.6498	−0.5016	1.3292	−0.3918	0.5128	0.1749
H	−0.6502	−0.5026	−1.3280	−0.3828	−0.7871	−1.1578
	$s_x = 0.0160$	$s_y = 0.0120$	$s_z = -0.4584$			
	$r = 1.4$	$R = 2.140$	$E = 2.916$	$\|\mathbf{t}^{IJ}\|$	$= 0.00011$	
Li	0.0000	1.3577	−0.0300	1.0987	−0.3572	1.3466
H	0.6995	−0.7820	1.3823	−0.7083	0.8100	−1.4085
H	−0.7005	−0.7816	−1.3532	−0.5963	−0.4537	−1.1440
	$s_x = 0.0380$	$s_y = 0.0073$	$s_z = -0.2425$			
	$r = 1.5$	$R = 2.504$	$E = 1.856$	$\|\mathbf{t}^{IJ}\|$	$= 0.00020$	
Li	0.0000	1.3577	−0.0342	1.6356	0.3973	1.3910
H	0.7496	−1.0314	0.1045	−1.2219	0.4981	−0.4332
H	−0.7504	−1.0312	−0.0710	−1.1185	−0.8962	−1.6625
	$s_x = -0.0501$	$s_y = -0.0059$	$s_z = -0.1282$			
	$r = 1.77$	$R = 2.969$	$E = 1.124$	$\|\mathbf{t}^{IJ}\|$	$= 0.00040$	
Li	0.0000	1.3577	0.0366	1.6824	−0.3715	1.3883
H	0.8846	−1.6117	0.2212	−1.7126	1.0064	−2.2529
H	−0.8854	−1.6115	−0.2586	−1.8353	−0.6358	−1.0009
	$s_x = -0.0503$	$s_y = 0.0477$	$s_z = -0.0018$			
	$r = 2.1$	$R = 3.591$	$E = 1.514$	$\|\mathbf{t}^{IJ}\|$	$= 0.00060$	
Li	0.0000	1.3577	−0.3088	1.1677	0.2014	1.0619
H	1.0495	−2.2338	1.5533	−2.6672	1.4288	−1.7412
H	−1.0506	−2.2334	−1.2456	−1.6100	−1.6853	−2.4302
	$s_x = 0.0387$	$s_y = 0.0591$	$s_z = 0.0420$			
	$r = 2.57$	$R = 4.426$	$E = 2.480$	$\|t^{IJ}\|$	$= 0.00073$	
Li	0.0000	1.3577	0.3514	1.4613	0.1056	1.0109
H	1.2843	−3.0687	0.9260	−2.5155	1.8385	−2.7136
H	−1.2857	−3.0683	−1.2788	−3.7251	−1.9454	−3.0767
	$s_x = 0.0160$	$s_y = 0.0531$	$s_z = 0.0467$			
	$r = 2.75$	$R = 4.740$	$E = 2.832$	$\|t^{IJ}\|$	$= 0.0007$	
Li	0.0000	1.3577	−0.0272	0.9932	0.3657	1.3306
H	1.3742	−3.3822	2.0184	−3.2469	1.2384	−2.7386
H	−1.3757	−3.3818	−1.9926	−3.1526	−1.6055	−3.9982
	$s_x = 0.0477$	$s_y = 0.0035$	$s_z = 0.0434$			
	$r = 3.0$	$R = 5.167$	$E = 3.263$	$\|t^{IJ}\|$	$= 0.0006$	
Li	0.0000	1.3577	−0.0301	0.9855	0.3654	1.3884
H	1.4992	−3.8099	2.1108	−3.5718	−0.0612	−0.0238
H	−1.5008	−3.8094	−2.1425	−3.6752	−1.6318	−4.4544
	$s_x = 0.0371$	$s_y = -0.0031$	$s_z = 0.0376$			
	$r = 3.25$	$R = 5.578$	$E = 3.622$	$\|t^{IJ}\|$	$= 0.00048$	
Li	0.0000	1.3577	0.0158	1.7473	−0.3674	1.3744
H	1.6241	−4.2203	0.9955	−4.3879	1.7811	−4.8593
H	−1.6259	−4.2197	−1.0131	−4.4417	−1.4154	−3.5974
	$s_x = 0.0274$	$s_y = -0.0012$	$s_z = 0.0319$			
	$r = 3.5$	$R = 5.961$	$E = 3.908$	$\|t^{IJ}\|$	$= 0.00034$	
Li	0.0000	1.3577	0.3701	1.3633	0.0051	0.9435
H	1.7491	−4.6037	1.5555	−3.9763	2.3558	−4.3878
H	−1.7509	−4.6032	−1.9275	−5.2362	−2.3627	−4.4047
	$s_x = 0.0003$	$s_y = 0.0189$	$s_z = 0.0266$			
	$r = 4.0$	$R = 6.633$	$E = 4.296$	$\|t^{IJ}\|$	$= 0.00015$	
Li	0.0000	1.3577	0.2299	0.9846	−0.3001	1.0721
H	1.9990	−5.2758	2.3431	−4.7081	−0.0344	−0.0568
H	−2.0010	−5.2752	−2.5750	−5.4698	−2.2027	−4.6349
	$s_x = 0.0056$	$s_y = 0.0043$	$s_z = 0.0170$			

Table 1. Contd.

Atom	x	y	h_x^{IJ}	h_y^{IJ}	g_x^{IJ}	g_y^{IJ}
	$r = 4.5$	$R = 7.216$	$E = 4.503$	$\|t^{IJ}\|$	$= 0.00005$	
Li	0.0000	1.3577	0.3351	1.6084	0.1960	0.9282
H	2.2489	−5.8588	1.7979	−5.4472	2.6348	−5.3299
H	−2.2511	−5.8581	−2.1352	−6.5204	−2.8330	−5.9574
	$s_x = 0.0010$	$s_y = 0.0017$	$s_z = 0.0092$			

Table 2. C_s portion of seam of conical intersection of Li + H_2 in Cartesian coordinates. $R_1 = R$ (Li − H^1), $R_2 = R$ (Li − H^2)

Atom	x	y	h_x^{IJ}	h_y^{IJ}	g_x^{IJ}	g_y^{IJ}
	$r = 1.270$	$R = 1.767$	$R_1 = 1.853$	$R_2 = 1.903$	$\gamma = 92.423°$	$E = 6.227$
Li	0.0000	0.0000	−0.0164	−0.2173	0.4241	−0.2597
H	0.6579	−1.7318	1.3475	−1.6114	0.3818	−1.0448
H	−0.6103	−1.8025	−1.2835	−1.7056	−0.7583	−2.2298
	$s_x = 0.0041$	$s_y = 0.2027$	$s_z = 0.5230$	$\|\mathbf{t}^{IJ}\|$	$= 0.000017$	
	$r = 1.274$	$R = 1.768$	$R_1 = 1.816$	$R_2 = 1.940$	$\gamma = 95.937°$	$E = 6.257$
Li	0.0000	0.0000	0.0331	−0.2202	−0.1439	−0.7675
H	0.6445	−1.6978	−0.0519	−1.8341	0.9012	−2.1739
H	−0.6219	−1.8376	0.0413	−1.9214	−0.7347	−2.1289
	$s_x = 0.0097$	$s_y = 0.5579$	$s_z = 0.0752$	$\|\mathbf{t}^{IJ}\|$	$= 0.000028$	
	$r = 1.289$	$R = 1.773$	$R_1 = 1.760$	$R_2 = 2.005$	$\gamma = 101.650°$	$E = 6.322$
Li	0.0000	0.0000	0.1120	0.7810	0.0575	0.1342
H	0.6227	−1.6457	0.6923	−2.1680	−0.1012	−1.7425
H	−0.6409	−1.8995	−0.8226	−2.1582	0.0254	−1.9370
	$s_x = 0.5535$	$s_y = 0.0420$	$s_z = 0.0286$	$\|\mathbf{t}^{IJ}\|$	$= 0.000060$	
	$r = 1.320$	$R = 1.783$	$R_1 = 1.693$	$R_2 = 2.090$	$\gamma = 108.573°$	$E = 6.468$
Li	0.0000	0.0000	0.1062	−0.7303	−0.0958	−0.3438
H	0.5952	−1.5849	0.2480	−1.1488	1.2749	−1.3406
H	−0.6644	−1.9811	−0.4233	−1.6870	−1.2483	−1.8816
	$s_x = 0.5722$	$s_y = 0.1345$	$s_z = 0.0404$	$\|\mathbf{t}^{IJ}\|$	$= 0.000088$	
	$r = 1.370$	$R = 1.800$	$R_1 = 1.626$	$R_2 = 2.185$	$\gamma = 115.576°$	$E = 6.725$
Li	0.0000	0.0000	0.1666	0.1202	−0.0590	0.8013
H	0.5655	−1.5246	−0.1990	−1.6501	0.6972	−1.9985
H	−0.6895	−2.0729	−0.0916	−2.0675	−0.7622	−2.4003
	$s_x = 0.0125$	$s_y = 0.6093$	$s_z = 0.1160$	$\|\mathbf{t}^{IJ}\|$	$= 0.000119$	
	$r = 1.386$	$R = 1.806$	$R_1 = 1.608$	$R_2 = 2.213$	$\gamma = 117.485°$	$E = 6.817$
Li	0.0000	0.0000	0.1815	−0.1615	0.0541	−0.1615
H	0.7536	−2.0804	1.3358	−2.0537	0.8643	−2.4083
H	−0.5158	−1.5230	−1.2794	−1.3881	−0.6806	−1.9901
	$s_x = 0.0292$	$s_y = 0.6168$	$s_z = 0.1339$	$\|\mathbf{t}^{IJ}\|$	$= 0.000128$	
	$r = 1.448$	$R = 1.827$	$R_1 = 1.552$	$R_2 = 2.306$	$\gamma = 123.330°$	$E = 7.717$
Li	0.0000	0.0000	−0.2676	−0.0435	0.1874	0.7742
H	0.5125	−2.2481	−0.0120	−2.1191	0.3456	−2.4981
H	−0.6636	−1.4030	1.1285	−1.48862	−0.6842	−1.9272
	$s_x = 0.1480$	$s_y = 0.6454$	$s_z = 0.1090$	$\|\mathbf{t}^{IJ}\|$	$= 0.000153$	
	$r = 1.470$	$R = 1.833$	$R_1 = 1.534$	$R_2 = 2.334$	$\gamma = 125.066°$	$E = 7.329$
Li	0.0000	0.0000	0.2016	0.4057	0.1284	−0.7019
H	0.5213	−1.4427	−0.1595	−1.7440	0.1157	−1.0522
H	−0.7276	−2.2183	−0.2484	−2.3227	−0.4504	−1.9069
	$s_x = 0.2537$	$s_y = 0.6063$	$s_z = 0.2166$	$\|\mathbf{t}^{IJ}\|$	$= 0.000178$	
	$r = 1.582$	$R = 1.872$	$R_1 = 1.461$	$R_2 = 2.474$	$\gamma = 132.331°$	$E = 8.081$
Li	0.0000	0.0000	−0.0078	0.0000	−0.7975	0.0000
H	0.4832	−1.3790	−0.3220	−1.4366	0.4686	−0.8361
H	−0.7626	−2.3540	−2.2886	0.0000	−2.0994	0.0000
	$s_x = 0.0942$	$s_y = 0.7338$	$s_z = 0.2207$	$\|\mathbf{t}^{IJ}\|$	$= 0.000206$	
	$r = 1.772$	$R = 1.940$	$R_1 = 1.369$	$R_2 = 2.687$	$\gamma = 141.028°$	$E = 9.466$
Li	0.0000	0.0000	0.1555	0.6495	0.3421	−0.4368
H	0.4308	−1.2999	−0.0042	−1.8194	−0.2558	−1.0235
H	−0.8152	−2.5608	−0.5358	−2.6908	−0.4708	−2.4003
	$s_x = 0.6492$	$s_y = 0.5699$	$s_z = 0.2536$	$\|\mathbf{t}^{IJ}\|$	$= 0.000262$	
	$r = 2.186$	$R = 2.096$	$R_1 = 1.231$	$R_2 = 3.109$	$\gamma = 152.727°$	$E = 12.639$
Li	0.0000	0.0000	0.7015	0.0000	−0.3301	0.0000
H	0.3410	−1.1831	0.7045	−1.7086	1.0660	−0.8708
H	−0.9194	−2.9697	−3.1457	0.0000	−2.9519	0.0000
	$s_x = 1.0562$	$s_y = 0.3016$	$s_z = 0.3395$	$\|\mathbf{t}^{IJ}\|$	$= 0.000457$	

References

1. Krauss M (1968) J Res Natl Bur Stand Sect A 72: 553
2. Companion AL (1968) J Chem Phys 48: 1186
3. Ruttink PJA, Lenthe JH van (1977) Theor Chim Acta 44: 97
4. Tully JC (1976) In: Miller WH (ed) Modern theoretical chemistry. Plenum, New York, pp 217–268
5. Botschwina P, Meyer W, Hertel IV, Reiland W (1981) J Chem Phys 75: 5438
6. Yusim YM, Lyast IT (1975) J Struct Chem 16: 463
7. Murav'eva NN, Baranovskii VI, Panin AI (1978) J Struct Chem 22: 8
8. Wagner AF, Wahl AC, Karo AM, Krejci R (1978) J Chem Phys 69: 3756
9. Mizutani K, Kuribara Y, Hayashi K, Matsumoto S (1979) Bull Chem Soc Jpn 52: 2184
10. Mizutani K, Yano T, Sekiguchi A, Hayashi K, Matsumoto S (1984) Bull Chem Soc Jpn 57: 3368
11. Toyama M, Uchide T, Yasyda T, Kasai T, Matsumoto S (1989) Bull Chem Soc Jpn 52: 2781
12. Mizutani K, Toyama M, Taguchi K, Matsumoto S (1985) Comput Chem 9: 259
13. Matsumoto S, Mizutani K, Sekiguchi A, Yano T, Toyama M (1986) Int J Quantum Chem 29: 689
14. Matsumoto S, Toyama M, Yasuda Y, Uchide T, Ueno R (1989) Chem Phys Lett 157: 142
15. Hobza P, Schleyer Pv R (1984) Chem Phys Lett 105: 830
16. Garcia-Prieto J, Feng, WL, Novaro O (1985) Chem Phys Lett 119: 128
17. Novaro O, Garcia-Prieto J, Pulain E, Ruiz M (1986) J Mol Struct (Theochem) 135: 79
18. Konowalow DD (1991) Preprint UDR-TR-91-36; AFAL/TSTR (STINFO). Edwards Air Force Base, Calif.
19. Chaban G, Gordon MS (1996) J Phys Chem 100: 95
20. Martinez TJ (1997) Chem Phys Lett 272: 139
21. Boldyrev AI, Simons J (1993) J Chem Phys 99: 4628
22. Clarke NJ, Sironi M, Raimondi M, Kumar S, Gianturco FA, Buonomo E, Cooper DL (1998) Chem Phys 233: 9
23. Jenkins DR (1968) Proc R Soc Lond Ser A 306: 413
24. Wu C (1979) J Chem Phys 71: 783
25. Elward-Berry J, Berry MJ (1980) J Chem Phys 72: 4510
26. Muller CH, Schofield K, Steinberg M (1980) J Chem Phys 72: 6620
27. Breckenridge WH, Umemoto H (1982) In: Lawley KP (ed) Advances in chemical physics: dynamics of the excited state, John Wiley, New York p 325
28. Hertel IV (1982) In: Lawley KP (ed) Advances in chemical physics, dynamics of the excited state p 475
29. Tully JC (1973) J Chem Phys 59: 5122
30. Fajardo ME (1993) J Chem Phys 98: 110
31. Scharf D, Martyna GJ, Klein ML (1993) J Chem Phys 99: 8997
32. Scharf D, Martyna GJ, Li D, Voth GA, Klein ML (1993) J Chem Phys 99: 9013
33. Cheng E, Whaley KB (1996) J Chem Phys 104: 3155
34. Werner HJ, Meyer W (1981) J Chem Phys 74: 5802
35. Atchity GJ, Ruedenberg K, Nanayakkara A (1997) Theor Chem Acc 96: 195
36. Chaban G, Gordon MS, Yarkony DR (1997) J Phys Chem A 101: 7953
37. Yarkony DR (1997) Theor Chem Acc 98: 197
38. Glezakou V-A, Gordon MS, Yarkony DR (1998) J Chem Phys 108: 5657
39. Yarkony DR (1997) J Phys Chem A 101: 4263
40. Born M, Huang K (1954) Dynamical theory of crystal lattices. Oxford University Press, Oxford
41. Berry MV (1984) Proc R Soc Lond Ser A 392: 45
42. Yarkony DR (1996) Rev Mod Phys 68: 985
43. Sidis V (1992) In: Baer M, Ng C-Y (eds) State-selected and state-to-state ion-molecule reaction dynamics, part 2 Wiley, New York, pp 73–134
44. Pacher T, Cederbaum LS, Köppel H (1993) Adv Chem Phys 84: 293
45. Mead CA, Truhlar DG (1982) J Chem Phys 77: 6090
46. McLachlan AD (1961) Mol Phys 4: 417
47. Hobeg WD, McLachlan AD (1960) J Chem Phys 33: 1695
48. Baer M (1975) Chem Phys Lett 35: 112
49. Macías A, Riera A (1978) J Phys B. 11: L489
50. Macías A, Riera A (1980) Int J Quantum Chem 17: 181
51. Petrongolo C, Buenker RJ, Peyerimhoff SD (1985) Chem Phys Lett 115: 249
52. Petrongolo C, Hirsch G, Buenker RJ (1990) Mol Phys 70: 825
53. Peric M, Buenker RJ, Peyerimhoff SD (1990) Mol Phys 71: 673
54. Peric M, Buenker RJ, Peyerimhoff SD (1992) Z Phys D 24: 177
55. Terao M, Harel C, Salin A, Allan RJ (1988) Z Phys D 7: 319
56. Alexander M (1993) J Chem Phys 99: 6014
57. Alexander M, Yang M (1995) J Chem Phys 103: 7956
58. Alexander MH (1998) J Chem Phys 108: 4467
59. Dobbyn AJ, Knowles PJ (1997) Mol Phys 91: 1107
60. Yarkony DR (1998) J Phys Chem A 102, 8073–8077
61. Matsunaga N, Yarkony DR (1998) Mol Phys 93: 79
62. Lengsfield BH, Yarkony DR (1992) In: Baer M, Ng C-Y (eds) State-selected and state to state ion-molecule reaction dynamics, part 2 Wiley New York, pp 1–71
63. Longuet-Higgins HC (1961) Adv Spectrosc 2: 429
64. Yarkony DR (1998) Acc Chem Res 31: 511
65. Senekowitsch J, H-J Werner, Rosmus P, Reinsch EA, ONeil SV (1985) J Chem Phys 83: 4661
66. Bartlett RJ (1995) In: Yarkony DR (ed) Modern electronic structure theory. World Scientific Singapore, p 1047–1131
67. Kendall RA, Dunning TH, Harrison RJ (1992) J Chem Phys 96: 6796
68. Moore CE (1971) Atomic energy levels, Natl Stand Ref Data Ser Natl Bur Stand. US GPO, Washington, DC
69. Errea Lf, Gorfinkel JD, Kryachko ES, Macías A, Mendez L, Riera A (1997) J Chem Phys 106: 172
70. Saxe P, Yarkony DR (1987) J Chem Phys 86: 321
71. Matsunaga N, Yarkony DR (1997) J Chem Phys 107: 7825
72. Kuntz PJ, Whitton WN, Paidarova I, Polak R (1994) Can J Chem 72: 939
73. Kolos W, Wolniewicz L (1968) J Chem Phys 49: 404